Journal of Advanced Zoology

ISSN: 0253-7214

*Volume **45** Issue **2Year 2024** Page **1389:1418***

Synthesis, ChracterizationAnd In- Vitro Studies On 2-Chloroquinolin In Derivatives As Anti- Alzheimer Disease.

Venkatachalm T[1*], Sojarna K[2], Senthil Kumar N.[3]

[1,2,3]Department of pharmaceutical chemistry, JKKMRF-Annai J.K.K Sampooraniammal college of pharmacy, Namakkal, Affliated to The Tamil Nadu Dr.M.G.R. Medical University, Chennai , Tamil Nadu - 638183.*

[1]Email id : venkatmohana301108@gmail.com, Phone number :+91 9843441716

[2]E mail id : deivamswamy@gmail.com, Phone number :+91 6374036954

[3]Email id : senthilkumarjkkm@gmail.com, Phone number :+91 9842024640.

***Corresponding Author:**Venkatachalm T*

Email id : venkatmohana301108@gmail.com, Phone number :+919843441716

Abstract

The synthesis, characterization and in-vitro studies on 2-chloroquinolin in derivatives have been screened and carried out by developing a QSAR model. Using such an approach one could predict the activities of newly designed compounds before a decision is being made whether these compounds should be really synthesized and tested. The data set used for the QSAR analyses contains 23 molecules belonging to acetyl cholinesterase inhibitors.About 20 novel compounds containing quinoline designed using CHEMDRAW software.Then the ten best docked compounds are selected for spectral data of the synthesized comopunds was obtained from IR, ^{1}H NMR, ^{13}C NMR, and mass spectroscopy,then the compounds are subjected to in-vitro MTT asssay for cell viability method.Amoung the tested compounds S9 and S11 were shown to be the most effective against the evaluated cell lines. Work is being done to advance the search for new cholinesterase inhibitors. In order to establish a SAR for rational study, more derivatives and in-depth, detailed investigations on in vivo activity may be undertaken. The current study suggests that more research is needed for quinoline derivatives developed as a potent lead for Anti-Alzheimer's disease.

Keywords:. acetyl cholinesterase inhibitors, QSAR analyses, Anti-Alzheimer's disease

INTRODUCTION

AD is a progressive, destructive neurodegenerative disorder. The main characteristics and clinical demonstrations of AD are cognitive impairment and memory loss, changes in mood and behavior, difficulty in performing familiar tasks, impairment in daily physical activities, in addition to a variety of neuropsychiatric symptoms [1]. The duration of the disease, during which the patient suffers from difficulty

in performing daily activities to the final stage of memory loss and immobility, is protracted, about 8–10 years [2].

The etiology of AD, leading to the neurodegeneration and destruction of neurons, is explained by several factors. The aggregation of beta-amyloid proteins (Ab), the destruction of cholinergic neurons, neuro-inflammation, mitochondrial damage, oxidative stress, and the degradation of tau proteins are the major predisposing factors for the progression of AD [3]. To date, the causes of neuro-degeneration in AD patients are not well understood, so effective and curative drugs cannot yet be developed [4]. The prominent neuronal alteration in AD is a change in the level of cholinergic neurotransmitters such as acetylcholine ACh concentration in the cortex and hippocampus. Studies on cholinergic neurons have shown that with disease progression, premature loss and severe damage to cholinergic neurons in the basal forebrain region can be observed [5]. Consequently, the inhibition of the AChE enzyme to prevent the hydrolysis of ACh is the most important strategy in the treatment of AD. Currently, the clinically used AChEI drugs only have symptom-relieving effects and improve the quality of life of patients in mild to moderate stages of the disease [6]. So far, there is no AChEI that can prevent the progression of the disease. In addition, AChEIs do not show the same pharmacological effect in all AD patients, and to date, it remains unclear why some patients respond while others do not [7]. According to some clinical studies regarding responders and non-responderstoAChEIs, it was reported that the probability of response to donepezil in patients with temporal lobe atrophy is very low, while patients with a high level of an allele known asAPOE-"4 are more likely to show a response to donepezil [8]. On the other hand,oxidative stress, characterized by the production of free radical reactive oxygen species(ROS), is one of the predisposing factors for the progression of AD. The overproductionof ROS plays an important role in the age-related progression of neurodegeneration andcognitive impairment [9].

QUINOLINE :

Quinoline is nitrogen containing heterocyclic aromatic compound known as 1-azanaphthalene, 1-benzazine or benzo[b] pyridine. As it is characterized by a double bond ring structure containing benzene fused to pyridine at adjacent carbon atoms. It has the formula C_9H_7N and has two isomers that is only difference in the position of nitrogen atom in the ring.

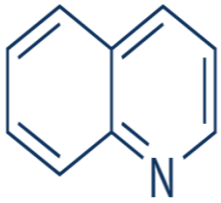

Quinoline derivatives represent as the major class of heterocycles and a number of preparations have been known since the late 1800s. The quinolone moiety is core structure of various natural products, especially in the alkaloids. The history of quinoline starts in 1820, when quinine (10) was isolated as the active ingredient from the bark of Cinchona trees and successively replaced the crude bark for the treatment of malaria. In spite of its moderately low efficacy and tolerability, quinine still plays an important role in the treatment of multiresistant malaria [10]. This molecule has also played a historical role in Organic Chemistry as a target for the structural determination and the total synthesis [11], recently in both stereoselective [12] and enantioselective [13] total syntheses. Chimanine alkaloids, simple quinolines (12-13), isolated from the bark of Galipealongiflora trees of the Rutaceae family [14-16], are effective against the parasites Leishmania species which are the agents for leishmaniasis, a protozoan diseases of the tropical areas in South America, particularly in the Amazonian forest. The quinoline derivatives show unique pharmaceutical activities such as antiplasmodial [18], intrinsic [19], cytotoxic [20], functional[21], antibacterial [22], antiproliferative [23], antimalarial [24] and anticancer activity [25]. Many tetrahydroquinoline derivatives investigated as drug candidates against type II diabetes [26], obesity [27], depression [28], inflammation [29] and heart failure [30]. Apart from these pharmaceutical activities, quinolines are important synthetic materials for the preparation of nano and mesostructures [31]. They are also used as catalyst, corrosion inhibitor, preservative and as a solvent for resins and terpenes. They are used in transition metal complex catalyst chemistry for

uniform polymerization, luminescence chemistry and as antifoaming agent in refinery field. The industrial, biological and synthetic significance places this scaffold at a prestigious position.

MATERIALS AND METHODS:

Oven dried glass wares were used to perform all the reactions. Procured reagents were of analytical grade and solvents of laboratory grade and purified as necessary according to techniques mentioned in Vogel's Textbook of Practical Organic Chemistry. In an open glass capillary tubes using Veego VMP-1 apparatus, melting points have been determined in ^{0}C and are uncorrected. Ascending TLC on precoated silica-gel plates (MERCK 6 F254) visualized under UV light was utilized to routinely monitor the progress and purity of the synthesized compounds. Solvents used during TLC are n-hexane, ethyl acetate, methanol, petroleum ether, chloroform and dichloromethane. The Infrared Spectra was plotted by Perkin-Elmer Fourier Transform-Infrared Spectrometer and in reciprocal centimetres the band positions are noted. Nuclear magnetic spectra (^{1}H NMR) were obtained from Bruker DRX-300 (500 MHz FT-NMR) spectrophotometer using DMSO as solvent with TMS as the internal standard^{13}C NMR have been recorded utilizing Bruker with Dimethyl sulphoxide as solvent. Shimadzu ESI-MS was employed to record Mass Spectra.

2D-QSAR APPROACH

Quantitative structure activity relationship (QSAR) relates the chemical structure to biological and other activities by developing a QSAR model. Using such an approach one could predict the activities of newly designed compounds before a decision is being made whether these compounds should be really synthesized and tested. The data set used for the QSAR analyses contains 23 molecules belonging to acetyl cholinesterase inhibitors. All the structures of the compounds were drawn in ChemDraw software. The structures of all the compounds along with their actual and predicted biological activities are presented in **Table 1**. A set of 23 molecules were selected and divided into training and test set in the ratio of 4:1. The negative logarithm of IC_{50} values (PIC_{50}) were calculated using the IC_{50} values of reported compounds. The compounds were run in the Padel software for descriptors generation. The descriptors along with the activity were proceeded for QSAR studies. QSARINS software is used for QSAR study. The data set is prepared by removing the constant variables greater than 80% and other correlated variables greater than 95% in the independent variables. Using genetic algorithm the QSAR model was developed. The models were validated in both internal and external validation. The models were verified by Applicbility domain. The applicability domain is used to identify the most influencing compound to the model. The leverage method and the insurbia graphs helps in identifying the outliers in this QSARINS software. Then the outliers were found and removed from the 1st model [51 – 52]. Then the remaining compounds were proceeded for next model generation in the same way.

Table 1. To idendify algorithm value for2D- QSAR analyses

Code	Structure	PIC_{50}
1	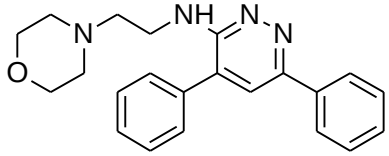	-5.414
2	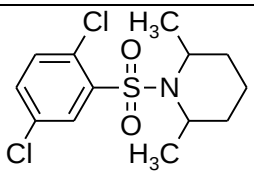	-1.875
3	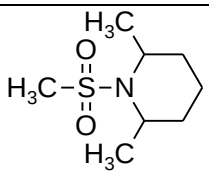	-1.929

4	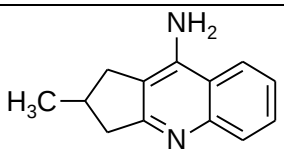	-1.785
5	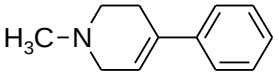	-6.143
6	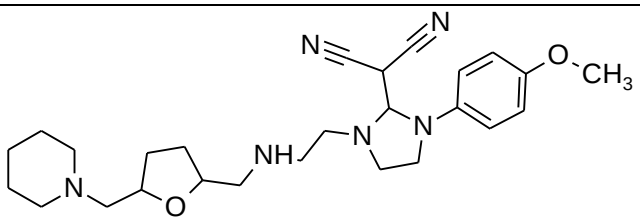	-1.278
7	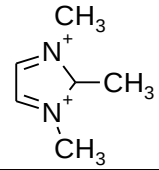	-5.079
8	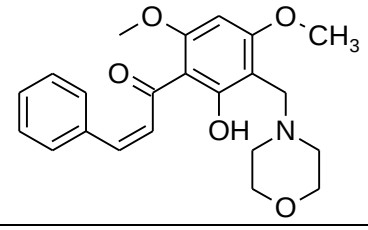	-5.423
9	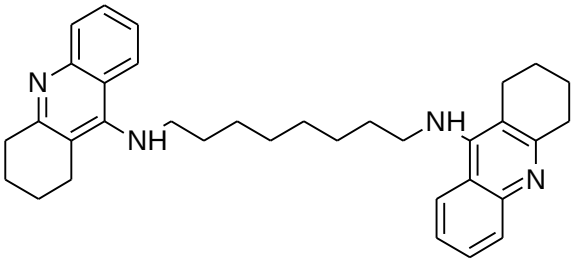	-1.154
10	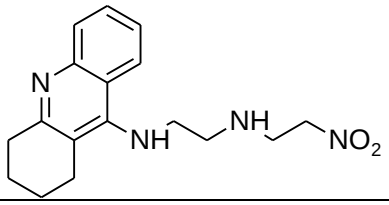	-0.863
11	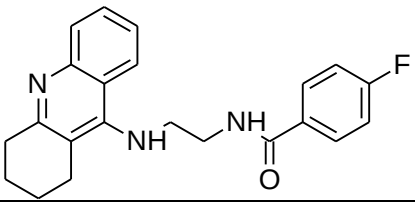	-0.578
12	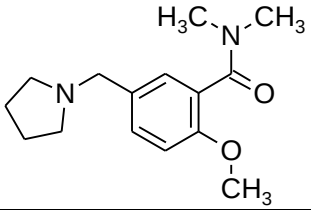	-1.462

13	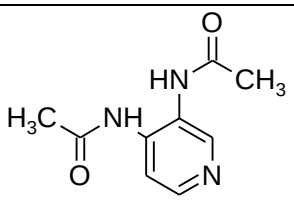	-5.605
14	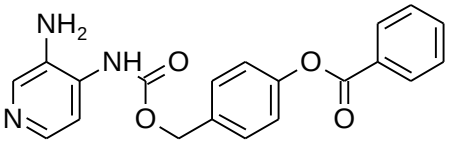	-5.593
15	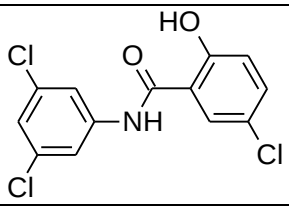	-1.66474
16	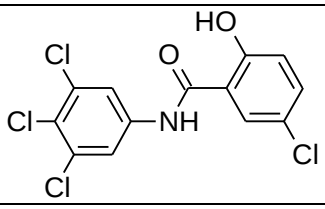	-1.70808
17	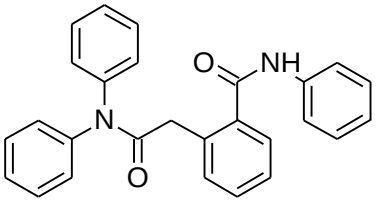	-1.7307
18	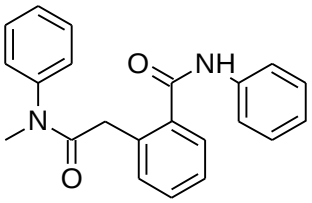	-1.74044
19	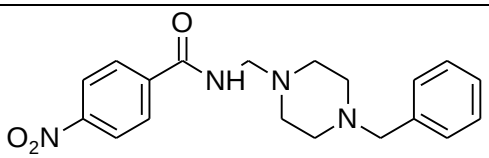	-0.83885
20	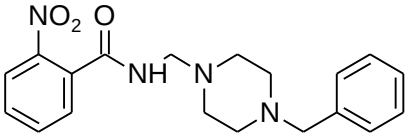	-1.36173
21	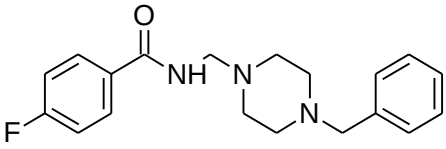	-0.60206
22	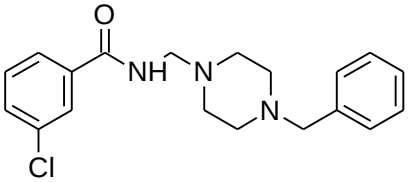	-0.95424

23	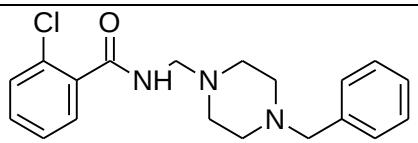	-0.98677

Compounds designing

About 20 novel compounds containing quinoline designed using CHEMDRAW software **(figure 1)**. CHEMDRAW is a drawing tool that allows you to draw chemical structures including organics, organometallics, polymers and Markush structures. It also includes features such as calculation of molecular properties (e.g. molecular weight, density, molar refractivity, etc.) 2D and 3D structure cleaning and viewing and functionality for naming structures.

In-silico molecular docking studies

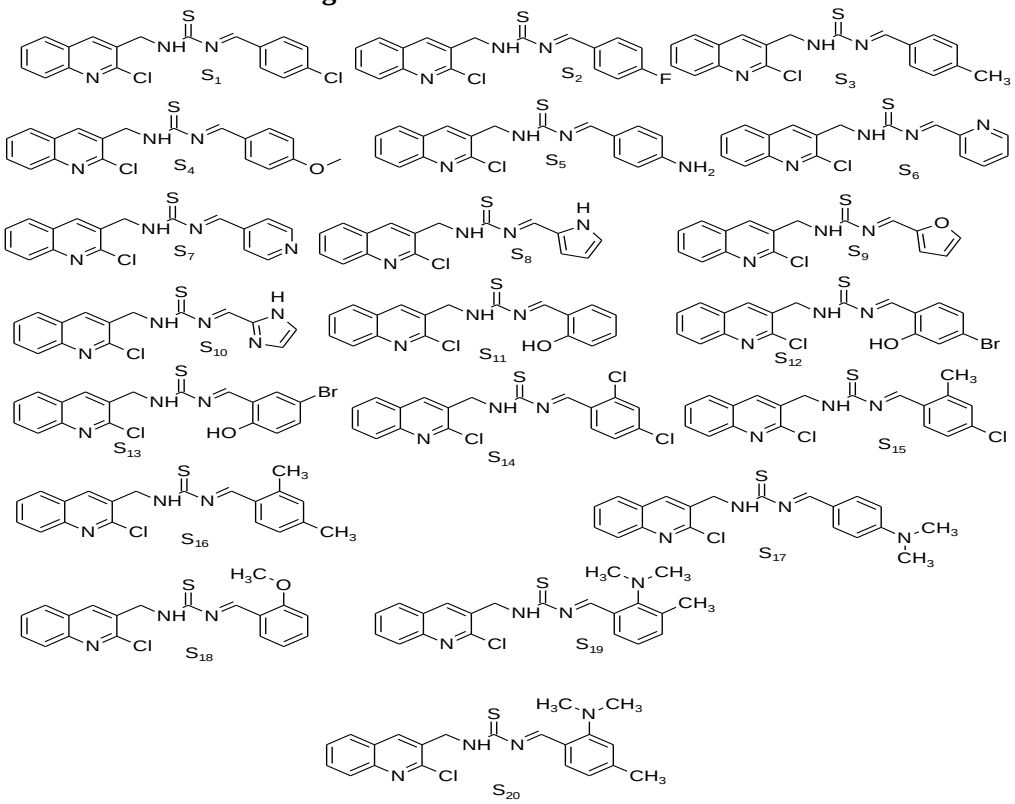

Devices and materials

In the molecular scenario in the modern drug design, the docking is commonly used to understand the interaction between the target ligand-receptor and the target lead molecule's binding orientation with its protein receptor and is quite frequently used to detect the associations between the target components. The research work was done *in-silico* by utilizing bioinformatics tools. Also, we utilize some of the online programming's like protein data bank (PDB) www.rcsb.org/pdb, PubChem database, Marvin sketch. The molecular docking studies were carried out through PyRx docking software.

Preparation of protein

By utilizing the offline program protein data bank (PDB), we take the Acetylcholinestrease(PDB ID: 1F8U) was obtained from PDB website. From the protein we removed the crystal water, followed by the addition of missing hydrogens, protonation, ionization, energy minimization. The SPDBV (swiss protein data bank viewer) force field was applied for energy minimization. Prepared protein is validated by utilizing the Ramachandran plot.

Identification of active sites

Identification of active amino acid present in the protein is detected by using Protein-ligand interaction profile (PLIP) https://plip-tool.biotec.tu-dresden.de/plipweb/plip/index online tool in google. From this, we found the active amino acid present in the protein.

Preparation of Ligands

By utilizing the Marvin sketch tool, the designed molecules are sketched in two and three-dimensional structures. After designed molecule, the structure was optimized in 3D optimization in Marvin sketch and saved as a pdb format.

Molecular Docking

We used PyRx virtual screening tool because it showed higher docking accuracy than other stages of the docking products (MVD: 87%, Glide: 82%, Surflex: 75%, FlexX: 58%) in the market coordinates in PDB format. Non- polar hydrogen atoms were removed from the receptor file and their partial charges were added to the corresponding carbon atoms. Molecular docking was performed using Molecular docking engine of PyRx software.

Chemistry

Step 1: synthesis of (E)-1-((2-chloroquinolin-3-yl) methylene) thiourea

The compound 2-chloroquinoline-3-carbaldehyde (2) was added with carbonyldiamide (3) in ethanol and was refluxed at 80-90°C for 5 hr to yield (E)-1-((2-chloroquinolin-3-yl) methylene) thiourea derivative.

Step2:Synthesisof3-[(2-chloroquinolin-3-yl)methyl]-1-[(1E)-phenylmethylidene]thiourea derivatives

The compound (E)-1-((2-chloroquinolin-3-yl) methylene) urea (4) was added with substituted aromatic aldehydes (5) and was refluxed at 80-90°C for 5 hr to yield the corresponding title compounds.

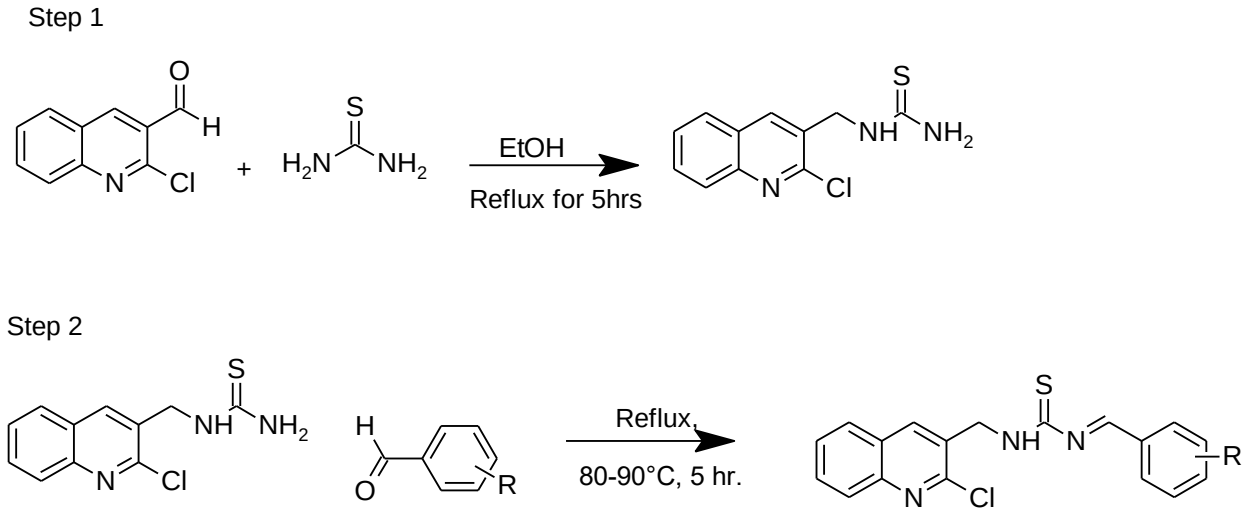

MTT assay for cell viability

Cell culture

Human SH-SY5Y neuroblastoma cells were purchased from sigma Aldrich and maintained in DMEM containing 10% FBS in a humidified atmosphere of 5.0% CO_2 in air at 37.0˚C. Experiments were performed at 80% confluence.

Determination of cell viability

Cell viability was assessed using a conventional MTT reduction assay as described previously [21], with some modifications. The assay was performed with three replicates. Cells at a density of 2.0 x 104 cells per well were placed in 96-well plates with 100 µL of fresh medium supplemented with 10% of FBS. After 24 h of stabilization, the cells were pretreated with five different concentrations of test compounds (25, 50, 100, 250 and 500 µg/mL, solubilized in DMEM plus 10% FBS) for 2 h. After 2 h, the treatment was combined with 10 µMAβ25–35 and incubated for another 24 h at 37.0˚C in 5.0% CO_2. A solvent control condition (DMEM + 10% FBS) was used as a control for the statistical analysis. After the treatment associated period, the culture medium was discarded and 100 µL of MTT (500 µg/mL) was added to all wells and the plates were incubated for 4 h. The MTT solution was then removed and 100 µL of DMSO was added to all wells to dissolve the dark blue crystals. The plates were shaken for a few minutes and read on a Thermo Plate reader (Thermo Plate, China) using a wavelength of 540 nm. Data were analysed and expressed as percentages relative to the control.

RESULT AND DISCUSSION

2D QSAR MODEL

2D QSAR models were generated to determine the structural relationship between the compounds and the acetylcholinesterase inhibition activity. The structures with their pIC50 value were given in the table. 1. About 2 models were generated and were listed below. The model 2 was found with the minimum number of outliers. So it was considered as the best. All the models were validated by both internal and external validation parameters. The experimental, predicted activities and leverage values were given in the table. 2.

MODEL 1

pIC50 = -1.3496 + 0.0162 (ATSC3i) - 0.7325 (GATS4i) -0.0509 (VE3_Dze) + 0.4199 (C3SP2)

R2: 0.8431 R2adj: 0.8327 R2-R2adj: 0.0105 LOF: 0.0553

Kxx: 0.3553 Delta K: 0.1138 RMSE tr: 0.2062 MAE tr: 0.1224

RSS tr: 2.7639 CCC tr: 0.9149 s: 0.2146 F: 80.6326

MODEL 2

pIC50 = -2.0963 + 0.1883 (AATSC4i) – 26.4482 (VE2_Dzi) +0.3572 (nBase) + 0.2309 (C3SP2) + 0.7007 (ETA_dBetaP)

R2: 0.9559 R2adj: 0.9517 R2-R2adj: 0.0042 LOF: 0.0125

Kxx: 0.3137 Delta K: 0.1292 RMSE tr: 0.0928 MAE tr: 0.0716

RSS tr: 0.5077 CCC tr: 0.9774 s: 0.0979 F: 229.5083

The model 2 is found to be best in statidtical parameters. The R2 value is 0.96 which is the co-efficient of correlation. This determines that the model is robust. The R2adj value is 0.9610 reveals that the model is convenient for the addition of another descriptor. The Friedman's Lack of fit is least saying that the model is not of chance correlation. The best model 2 is given in the Figure 2. Internal validation by cross validation leave-one-out (Q2LOO) was carried out and the value stood nearer to R2 value of the model.

In model 2, the R2Yscr and Q2Yscr value are 0.0926 and -0.1513 respectively. These values are in decreased state to that of the R2 and Q2 value of the model 2. Thus model 2 is not by chance correlation. In the same manner the descriptors were varied randomly and model was calculated. This is known as the Y-scramble for the descriptors. r2Yrnd and Q2Yrnd values are 0.0905 and -0.1540 respectively, which is decreased than the model r2 and Q2 values. (Figure.2)

Table 2. Experimental, predicted activities, leverage values of all the models and their residues.

Name	Exp. endpoint	Pred. activity model 1	Residual value: model 1	Pred. activity model 3	Residual value: model 3	HAT value model 1 (h*=0.3273)	HAT value model 3 (h*=0.3273)
1	-1.6964	-1.8171	-0.1206	-1.6601	0.0364	0.0389	0.1143
2	-1.7745	-1.8008	-0.0262	-1.7489	0.0257	0.0363	0.0586
3	-1.8838	-1.8251	0.0587	-1.7844	0.0994	0.0414	0.0692
4	-1.7838	-1.7545	0.0293	-1.8145	-0.0307	0.0365	0.0594
5	-1.6647	-1.7127	-0.048	-1.6752	-0.0105	0.0411	0.1039
6	-1.7081	-1.5426	0.1655	-1.745	-0.0369	0.123	0.0635
7	-1.6992	-1.8292	-0.13	-1.833	-0.1337	0.0464	0.1129
8	-1.7653	-1.8423	-0.077	-1.7896	-0.0243	0.0465	0.0576
9	-1.7683	-1.6697	0.0986	-1.7444	0.0239	0.0691	0.0555
10	-1.6837	-1.7226	-0.039	-1.8195	-0.1358	0.0593	0.0594
11	-1.7357	-1.6421	0.0935	-1.6962	0.0395	0.062	0.0622
12	-1.7669	-1.7652	0.0017	-1.7359	0.031	0.0489	0.052
13	-1.7005	-1.6711	0.0295	-1.6416	0.0589	0.1481	0.1424
14	-1.764	-1.7822	-0.0182	-1.7073	0.0568	0.0375	0.1425
15	-1.7497	-1.8169	-0.0673	-1.7428	0.0069	0.0408	0.0731
16	-1.6652	-1.7108	-0.0456	-1.7894	-0.1242	0.0486	0.0764
17	-1.7003	-1.5856	0.1147	-1.6502	0.0501	0.1026	0.2316
18	-1.7618	-1.7111	0.0507	-1.7325	0.0293	0.062	0.1175
19	-1.7784	-1.8126	-0.0342	-1.7841	-0.0057	0.0499	0.2968
20	-1.7658	-1.8351	-0.0693	-1.7407	0.0251	0.0472	0.0993
21	-1.7838	-1.6417	0.1421	-1.7312	0.0526	0.0594	0.1062
22	-1.7983	-1.7071	0.0912	-1.8063	-0.008	0.049	0.0604
23	-1.8343	-1.1455	0.6888	-	-	0.6141	-

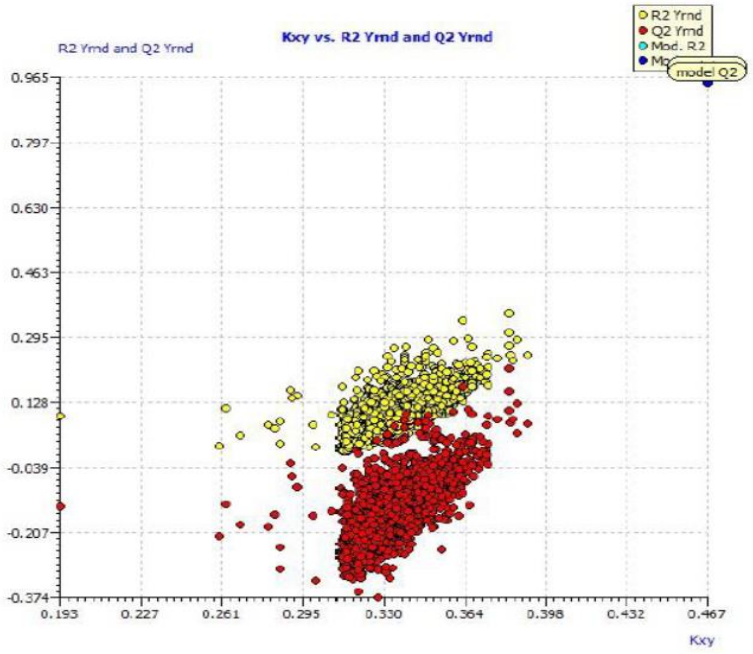

Figure 1. Y-scrambling by varying the descriptors for the model 2

Molecular docking

The molecular docking studies for the designed compounds were carried out through PyRx molecular docking software to determine the free energy binding towards targeted enzymes. The docking pose for the ligand enzyme interaction was visualized with discovery studio. The binding free energy for all the ligands was tabulated in table 3. From the results it clearly shows that, all the compounds have promising interaction with targeted enzyme AChE. The interaction is mainly due to the presence of lipophilic factor of aromatic heterocyclic ring. From the docking results, compound S7 (-9.3 kcal/mol) shows highest binding affinity toward AChE enzyme compared to standard drug donepezil. This compound produced five conventional hydrogen bonds between carbonyl oxygen, acid oxygen from hydroxyl group and nitrogen of triazole moiety with residues of Arg 133, Glu 249, Pro 647, Gln 648 and Try 731 respectively. The remaining the entire studied compound shows good to moderate binding affinities to the selected enzymes. These amino acids have been repeatedly implicated during ligand interaction with the AChEand also play important role in the inhibition of the ligand-binding domain of AChEinhibitors. These non-covalent interactions, van der Waals, columbic interaction, π–π interaction, and hydrogen interaction, are shown in **Figure 2 to 11**. The table 3 shows the binding energy of studied compounds. Based on the docking score the following derivatives like S2, S3, S5, S6, S7, S8, S9, S10, S11 and S18 are selected for the conventional synthesis and it was further evaluated for the in vitro activity using corresponding cell line.

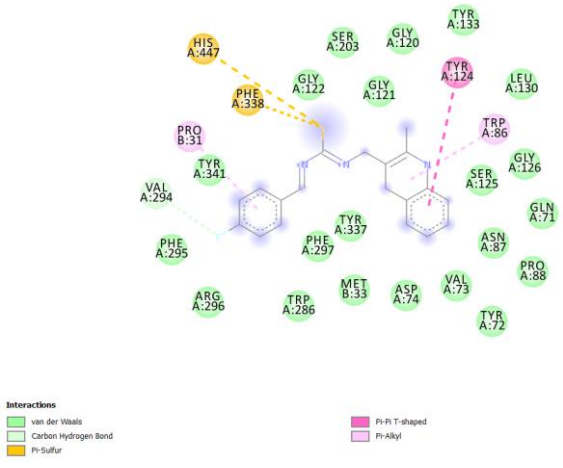

Figure 2. 2D docking interaction of compound S2 against AChEenzyme

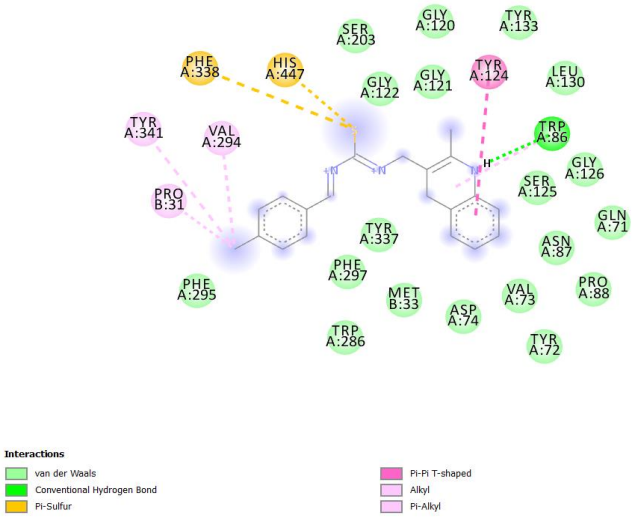

Figure 3. 2D docking interaction of compound S3 against AChEenzyme

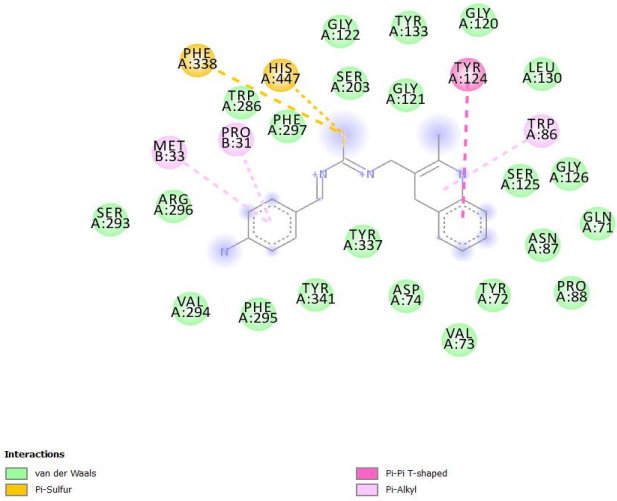

Figure 4. 2D docking interaction of compound S5 against AChEenzyme

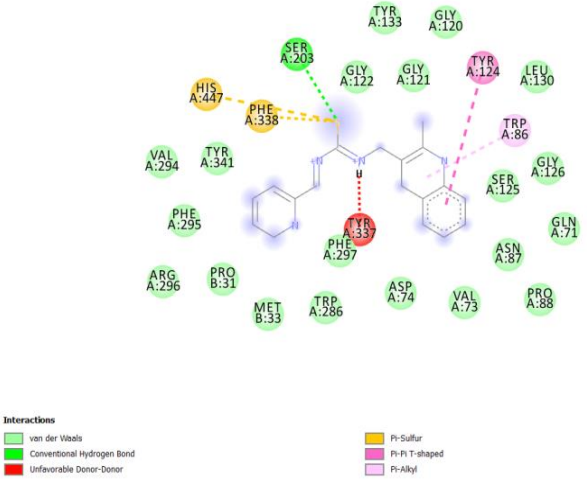

Figure 5. 2D docking interaction of compound S6 against AChEenzyme

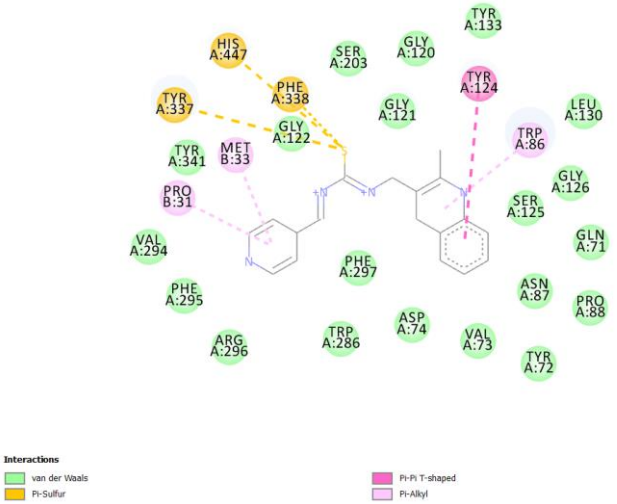

Figure 6. 2D docking interaction of compound S7 against AChEenzyme

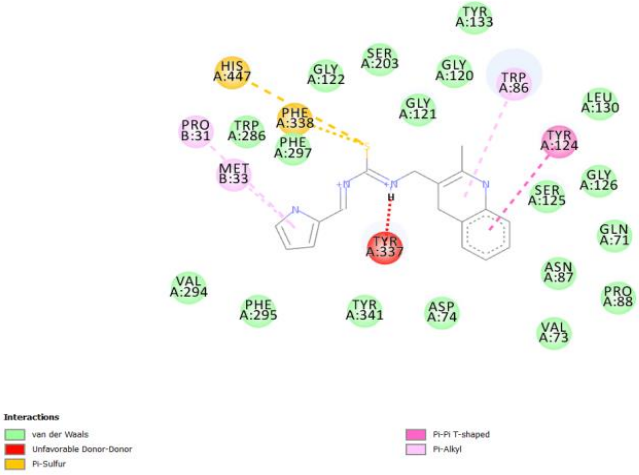

Figure 7. 2D docking interaction of compound S8 against AChEenzyme

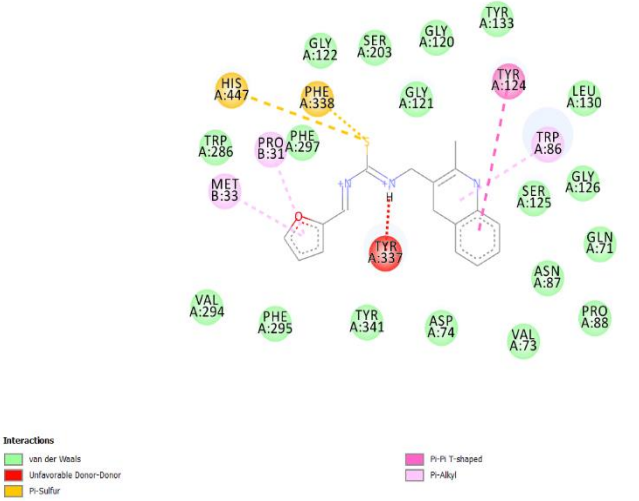

Figure 8. 2D docking interaction of compound S9 against AChEenzyme

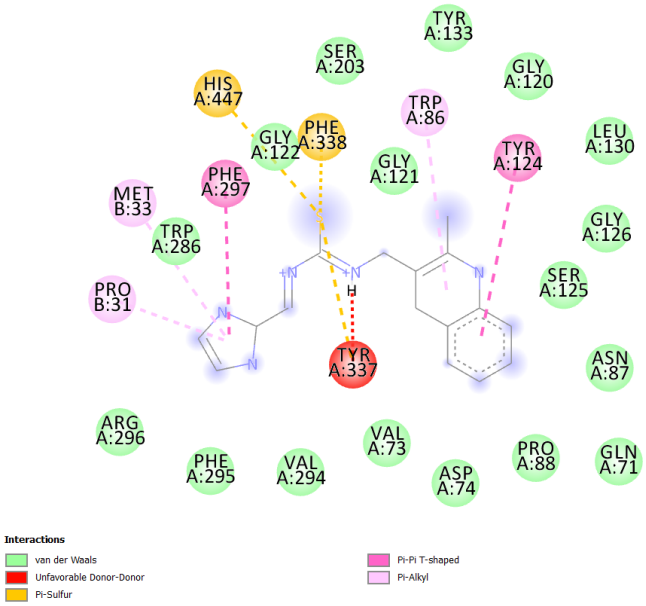

Figure 9. 2D docking interaction of compound S10 against AChEenzyme

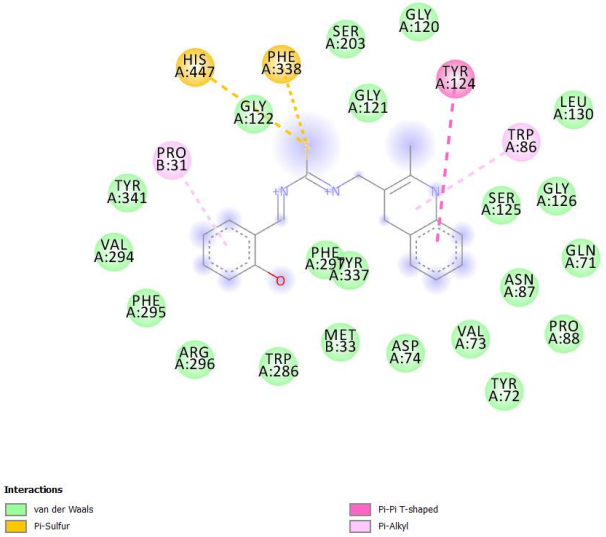

Figure 10. 2D docking interaction of compound S11 against AChEenzyme

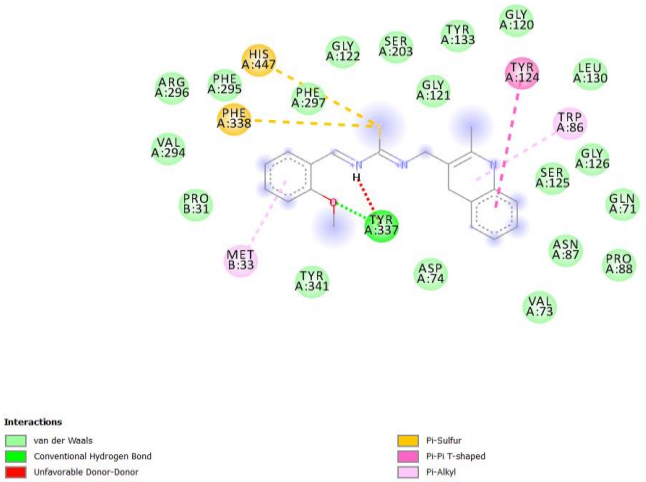

Figure 11. 2D docking interaction of compound S18 against AChE enzyme.

Table 3. Binding energy of studied compounds.

Ligand	Binding Affinity
S1	-7.1
S2	-7.4
S3	-8.8
S4	-7.7
S5	-8.6
S6	-9.2
S7	-9.3
S8	-9.1
S9	-9.1
S10	-8.3
S11	-9.2
S12	-7.6
S13	-7.3
S14	-7.7
S15	-8.1
S16	-8.1
S17	-7.4
S18	-8.2
S19	-6.7
S20	-8.1
Donepezil	-11.2

Chemistry

The final derivatives of derivatives were achieved by two step process. The compound 2-chloroquinoline-3-carbaldehyde (2) was added with carbonyldiamide (3) in ethanol and was refluxed at 80-90°C for 5 hr to yield (E)-1-((2-chloroquinolin-3-yl) methylene) thiourea derivative. The compound (E)-1-((2-chloroquinolin-3-yl) methylene) urea (4) was added with substituted aromatic aldehydes (5) and was refluxed at 80-90°C for 5 hr to yield the corresponding title compounds.The completion of the reaction and purity of synthesized compounds were analyzed by TLC using ethylacetate and n-hexane as mobile phase and the synthesized derivatives was subjected to melting point determination. The structure of synthesized compounds was elucidated by various spectral analyses. From the spectral analysis, it evident that all the compounds showed a corresponding signals in all the spectral data. The spectral data for all the compounds are given below:

Spectral Data of synthesized compounds

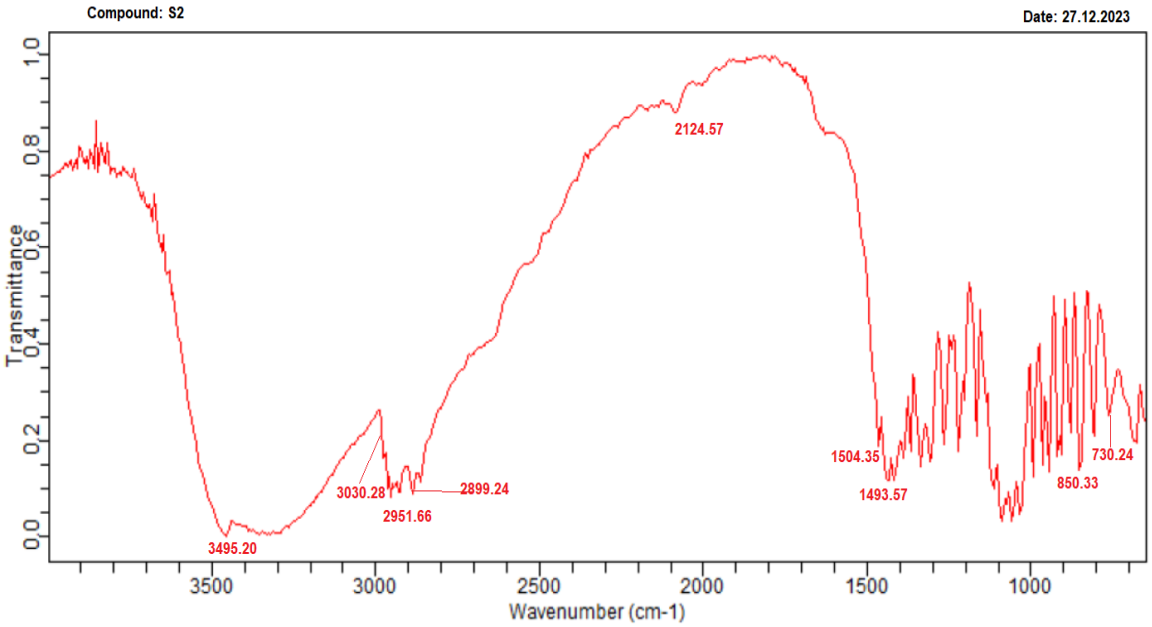

Figure 12: IR Spectra for compound S2

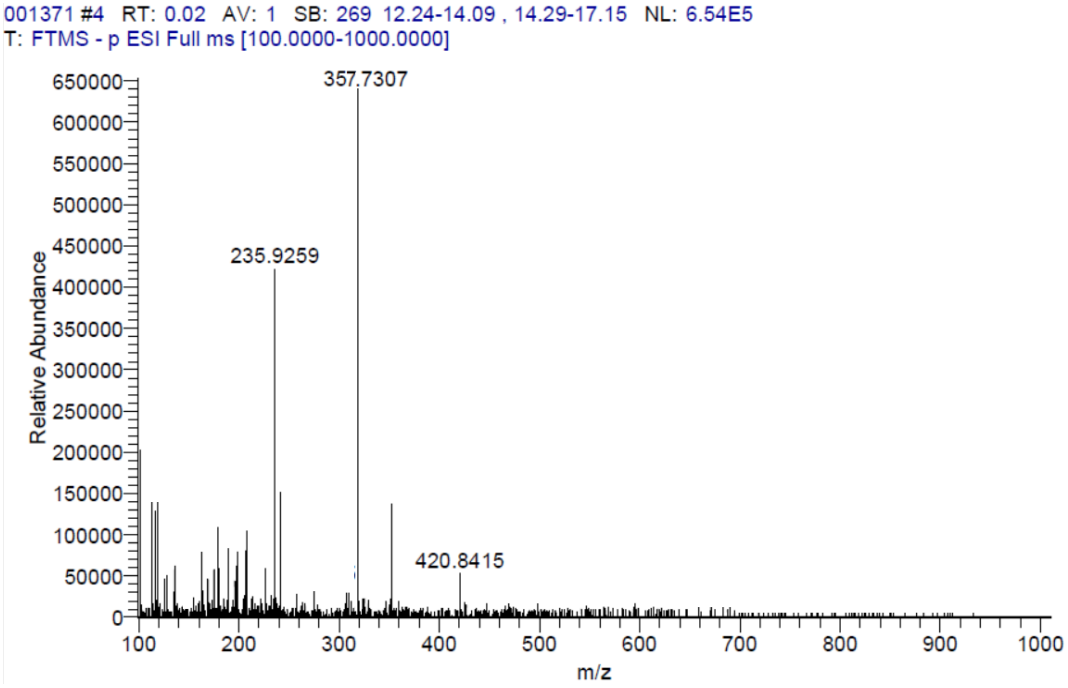

Figure 13: Mass Spectra for compound S2

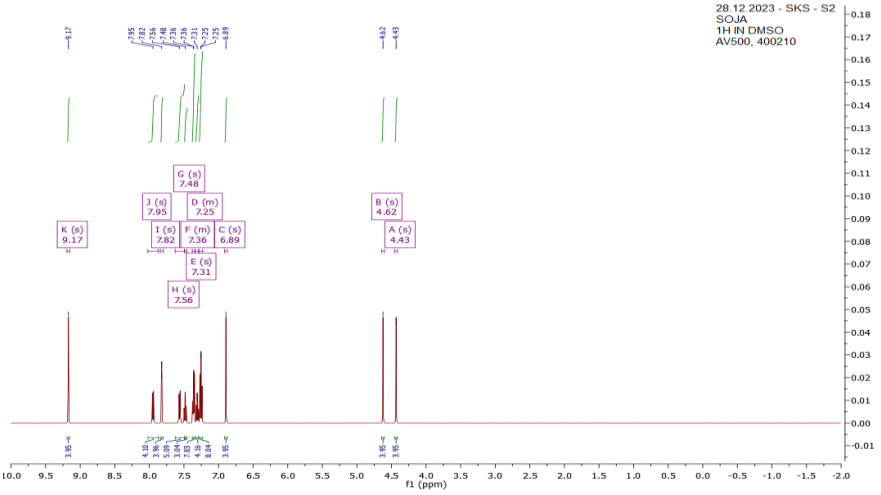

Figure 14: [1]H NMR Spectra for compound S2

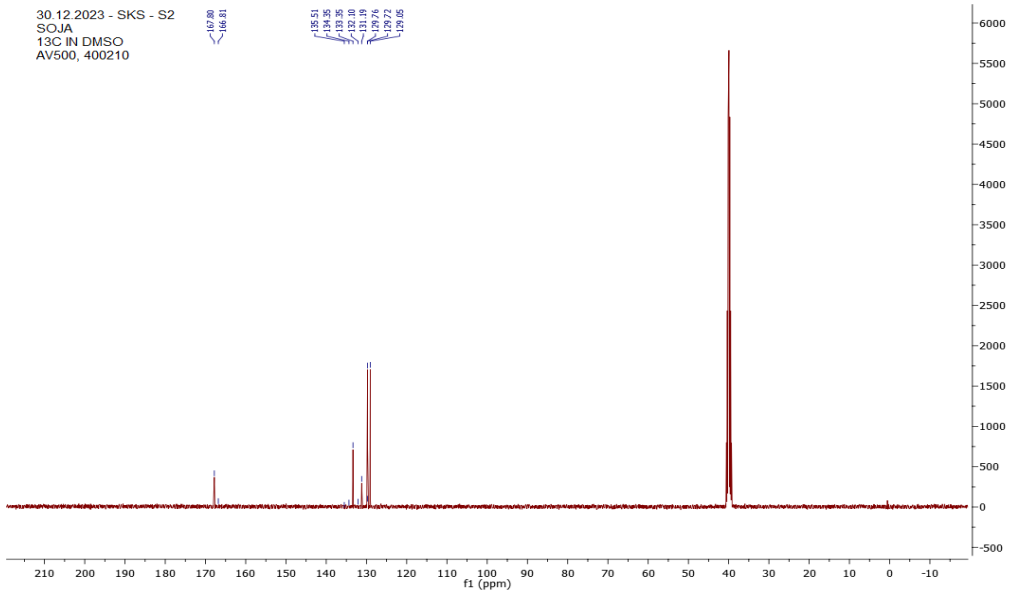

Figure 15: [13]C NMR Spectra for compound S2

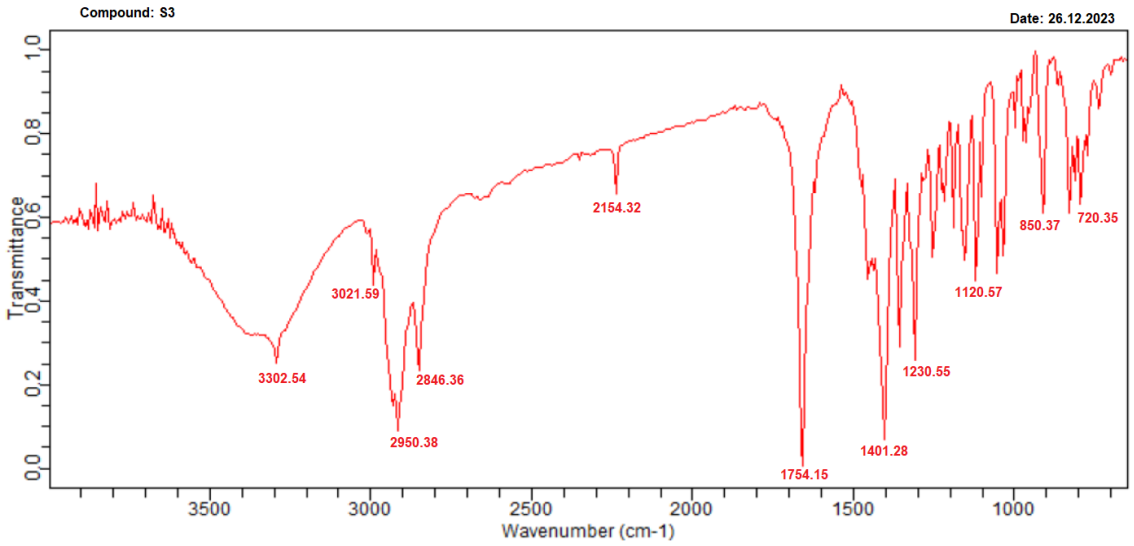

Figure 16: IR Spectra for compound S3

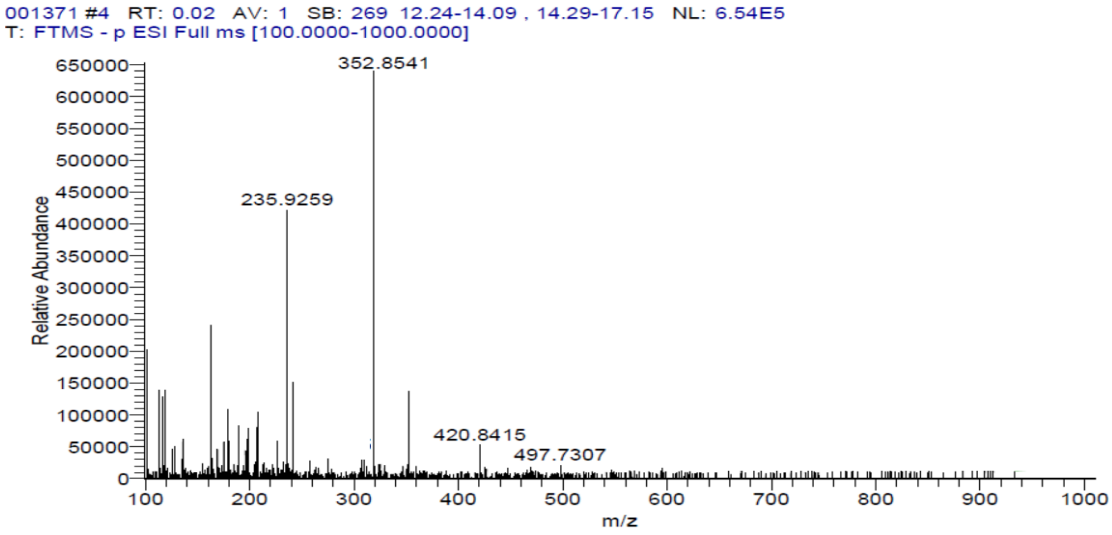

Figure 17: Mass Spectra for compound S3

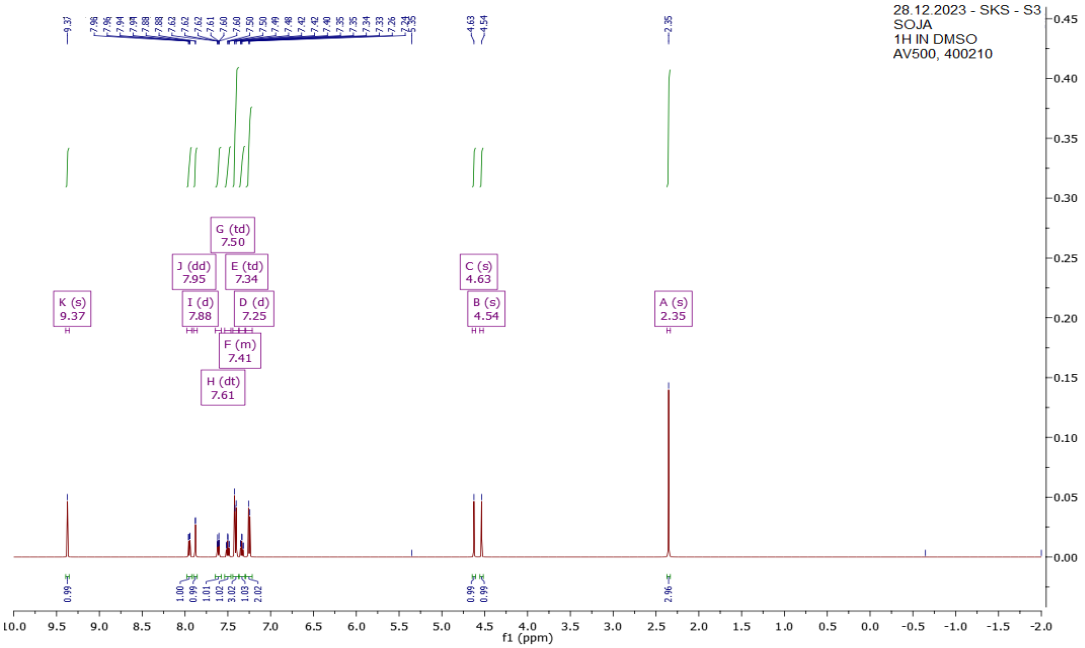

Figure 18: ^{1}H NMR Spectra for compound S3

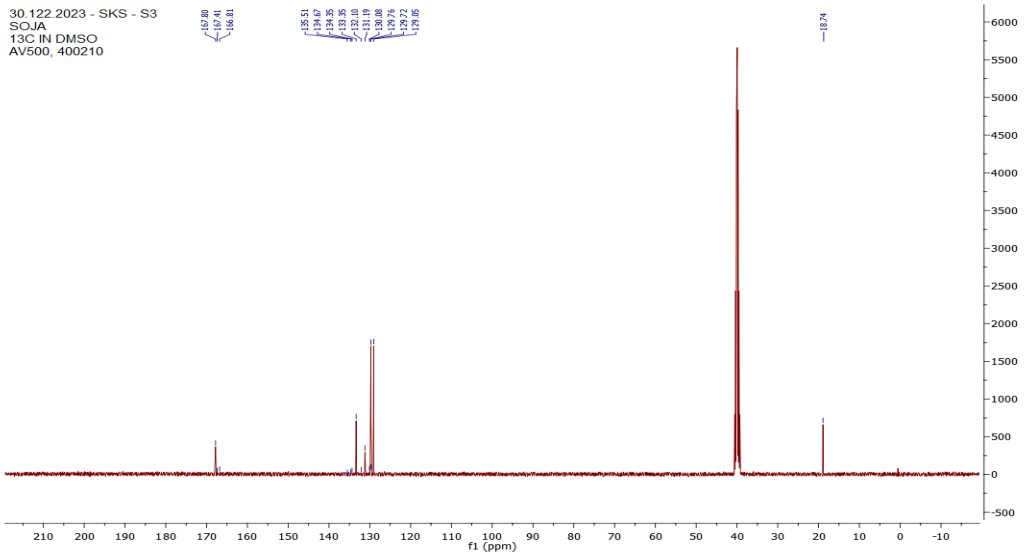

Figure 19: ^{13}C NMR Spectra for compound S3

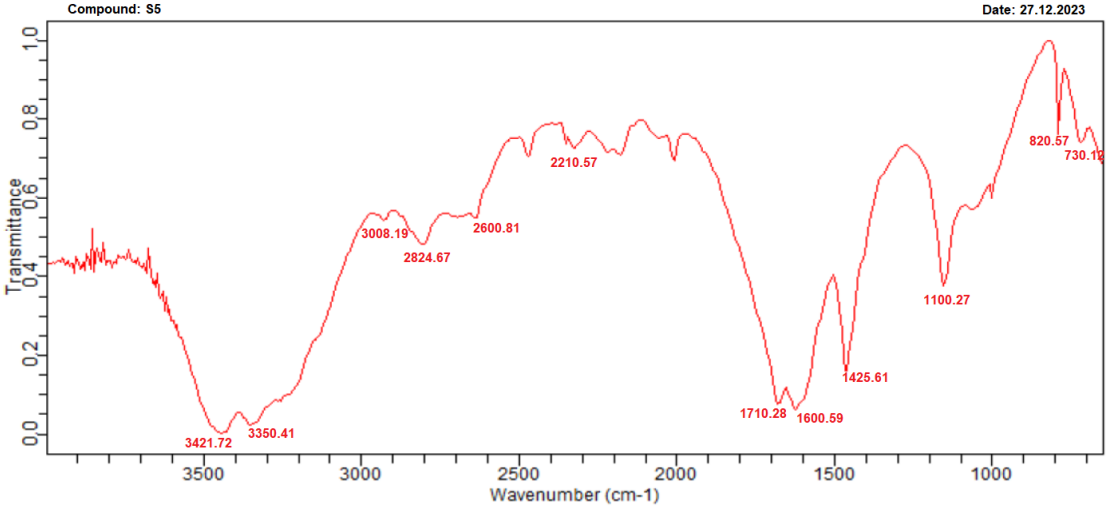

Figure 20: IR Spectra for compound S5

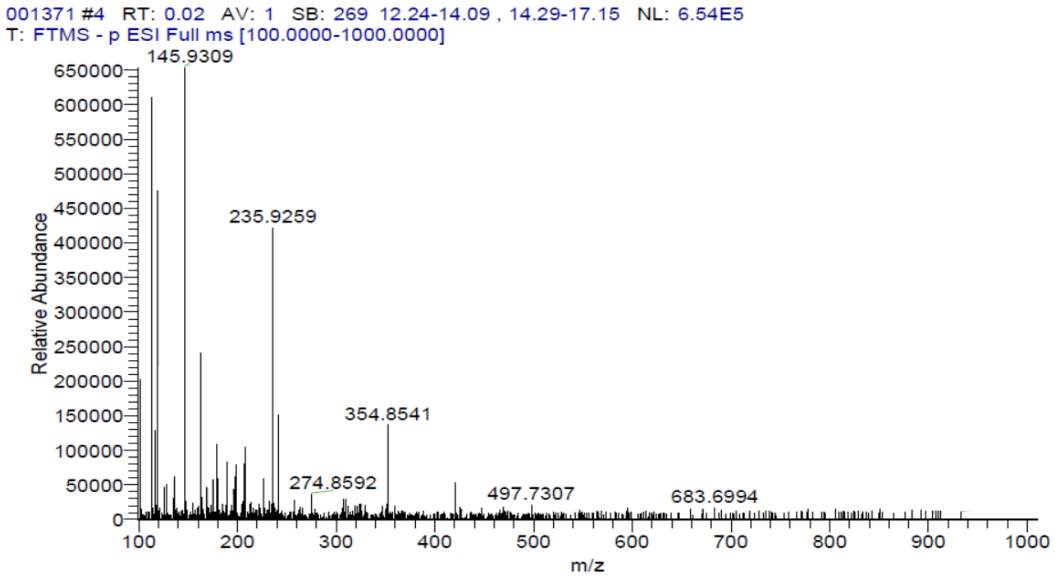

Figure 21: Mass Spectra for compound S5

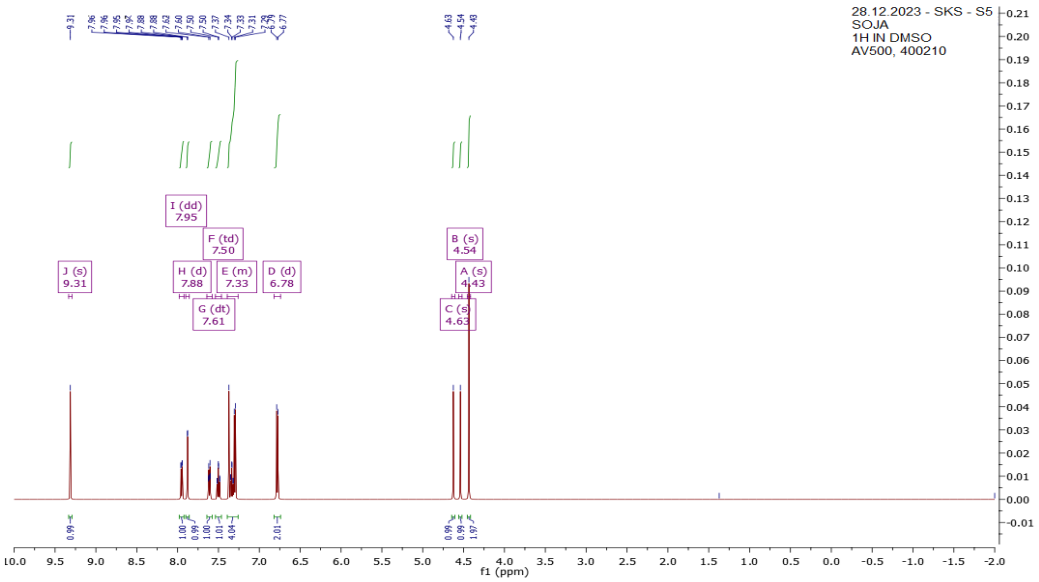

Figure 22: ^{1}H Spectra for compound S5

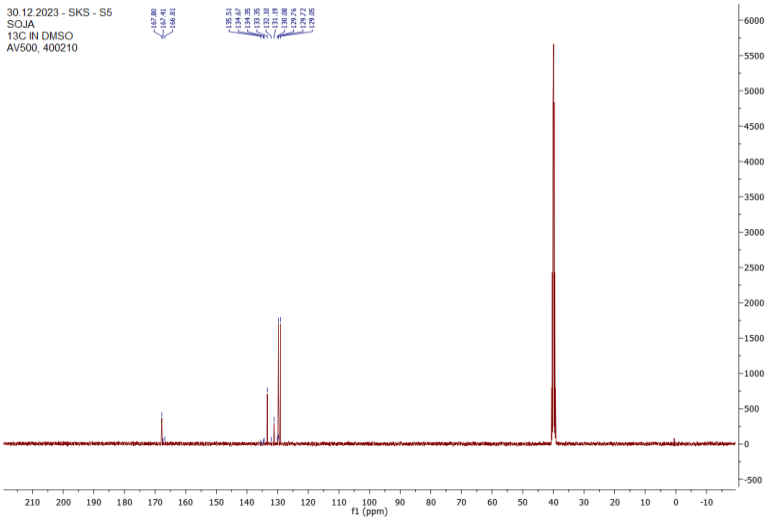

Figure 23: ^{13}C NMR Spectra for compound S5

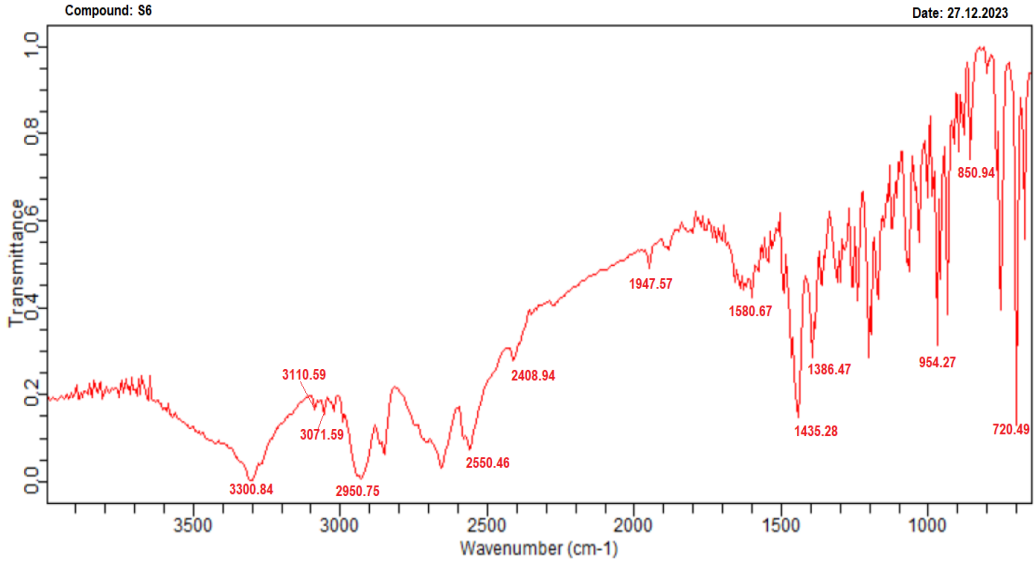

Figure 24: IR Spectra for compound S6

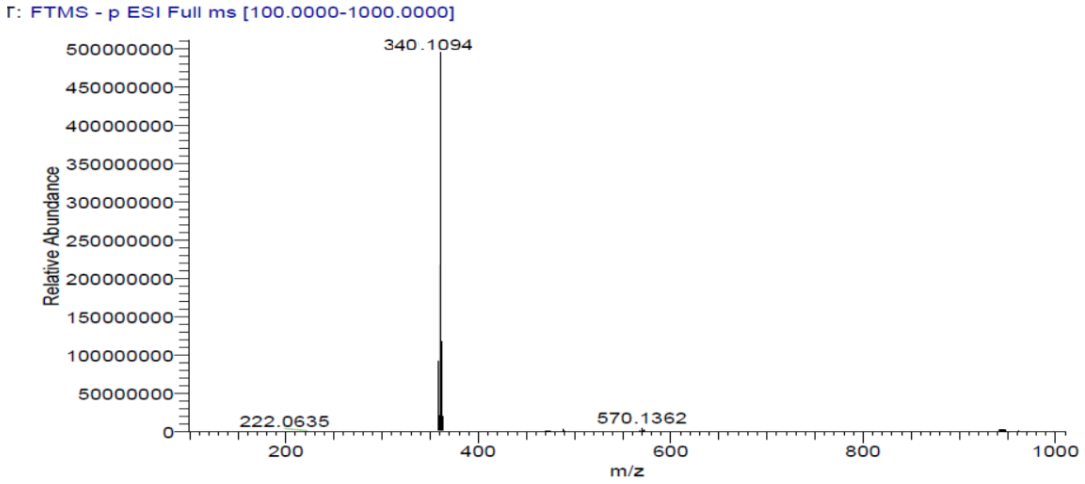

Figure 25: Mass Spectra for compound S6

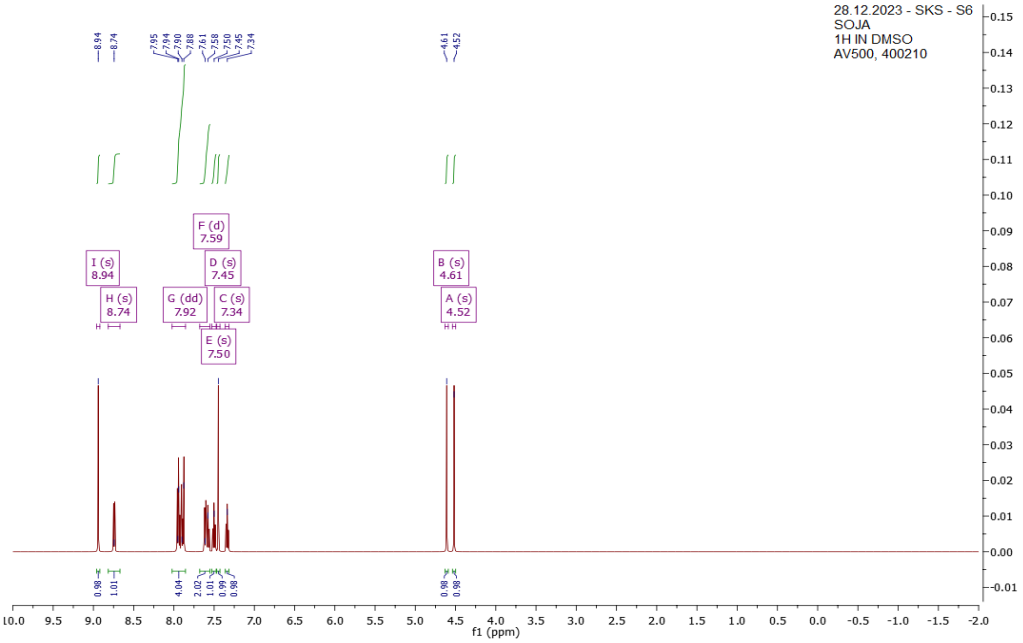

Figure 26: ^{1}H NMR Spectra for compound S6

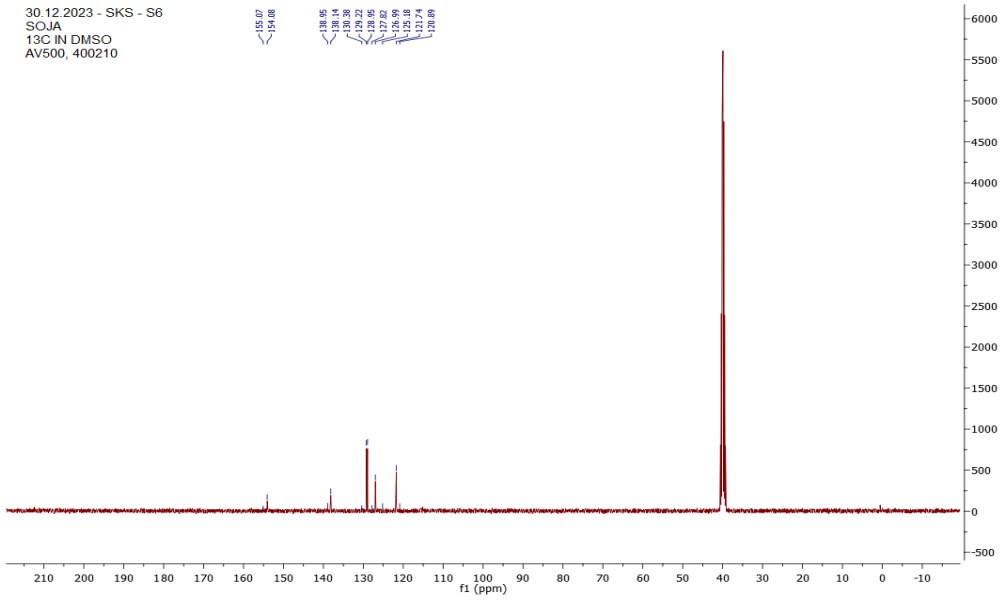

Figure 27: ^{13}C NMR Spectra for compound S6

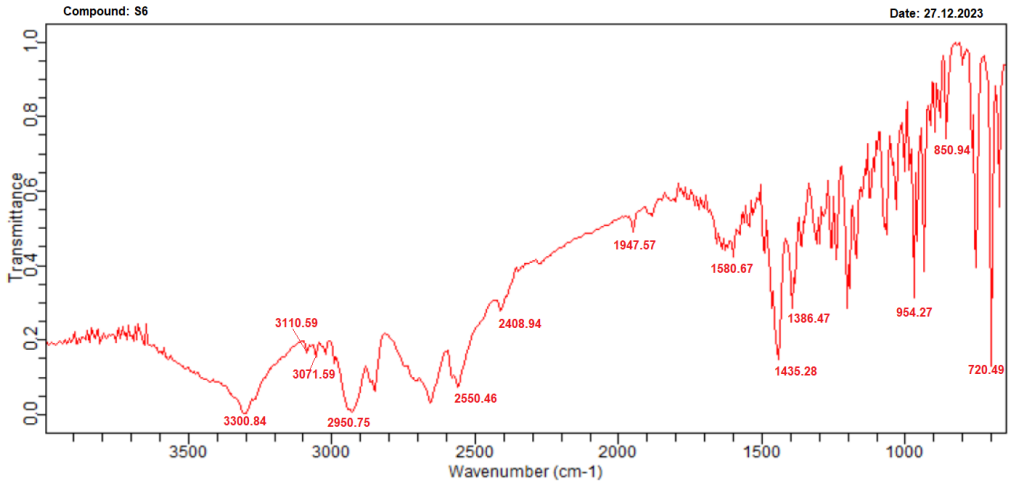

Figure 28: IR Spectra for compound S7

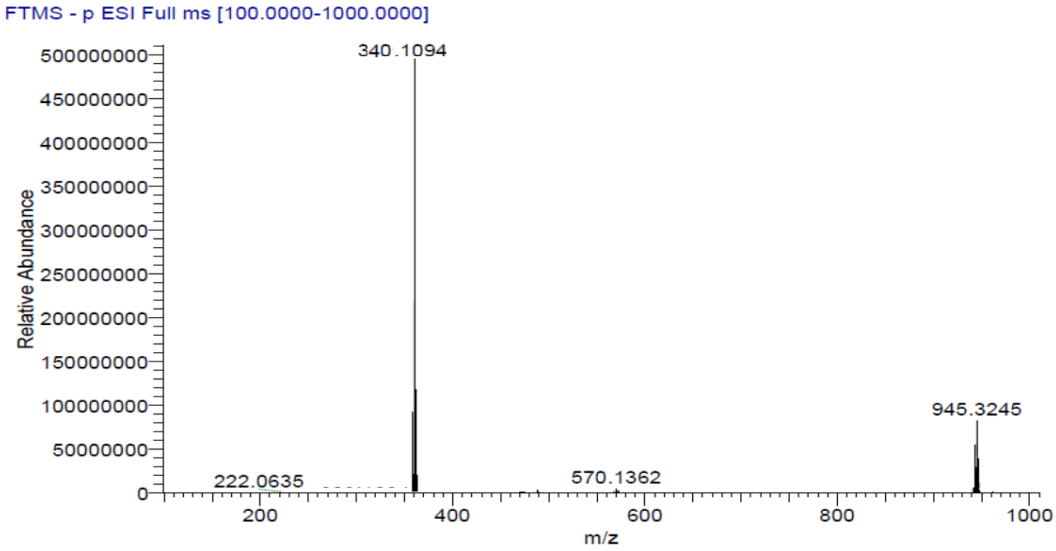

Figure 29: Mass Spectra for compound S7

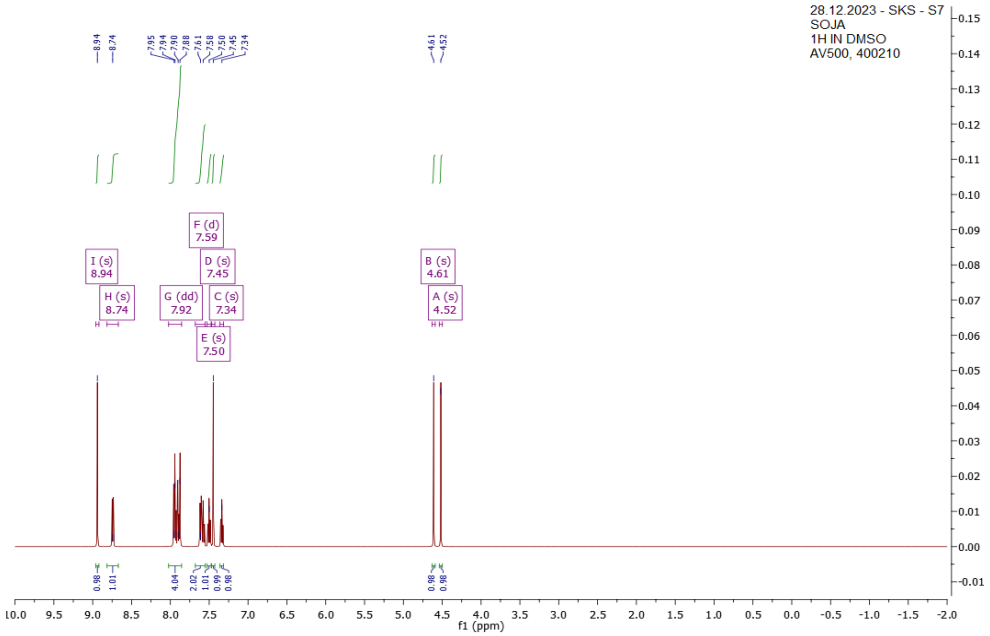

Figure 30: ^{1}H NMR Spectra for compound S7

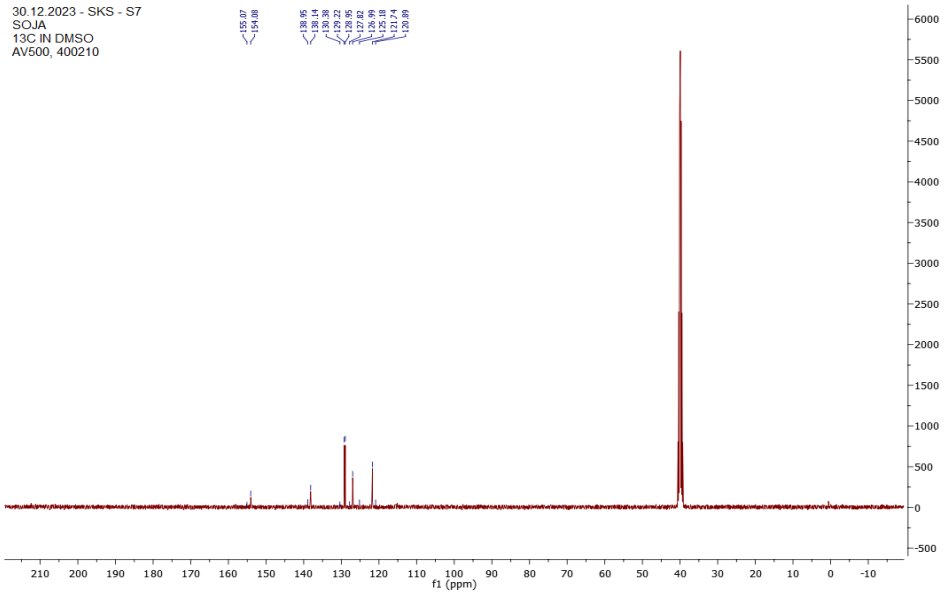

Figure 31: ^{13}C NMR Spectra for compound S7

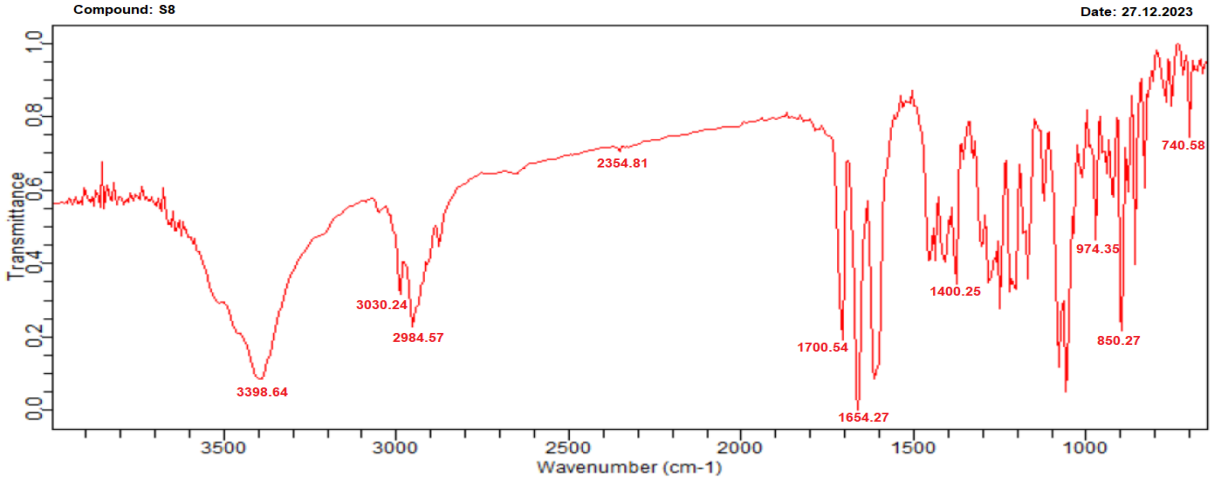

Figure 32: IR Spectra for compound S8

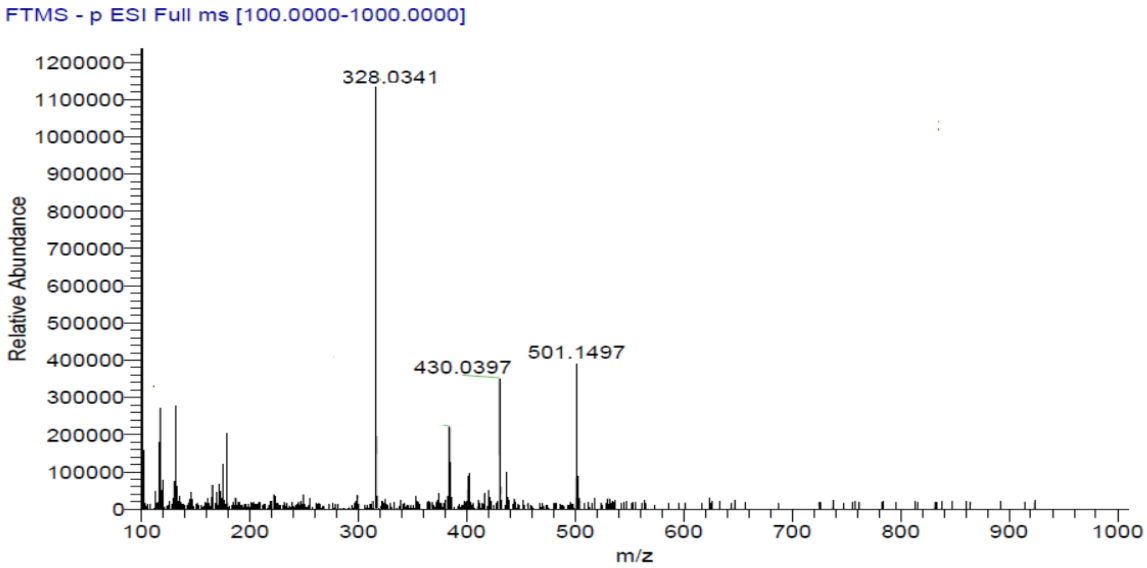

Figure 33: Mass Spectra for compound S8

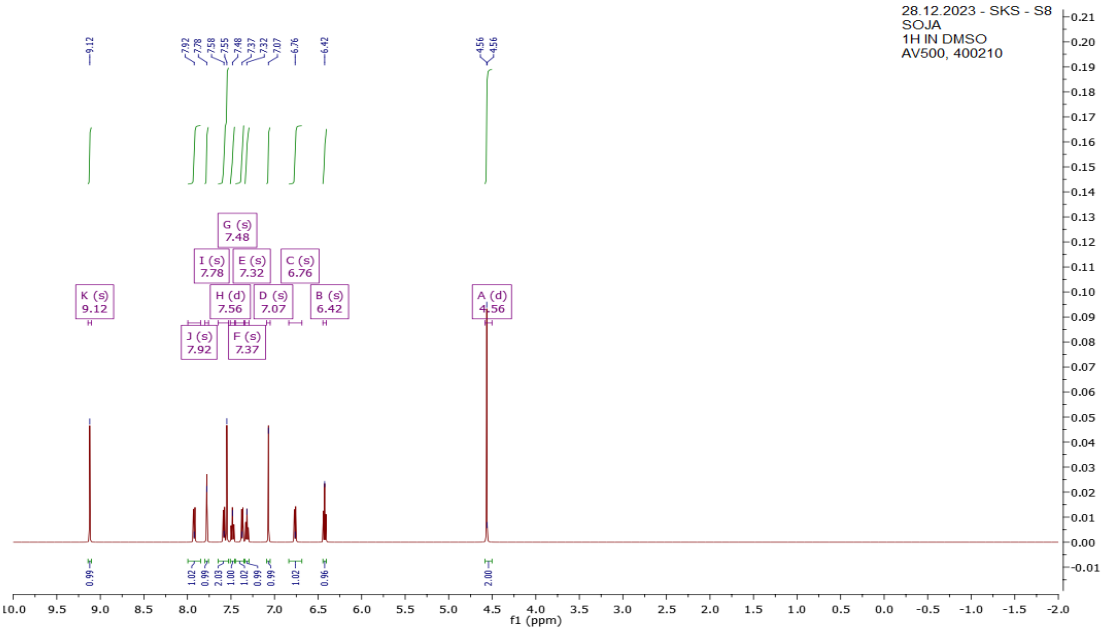

Figure 34: ^{1}H NMR Spectra for compound S8

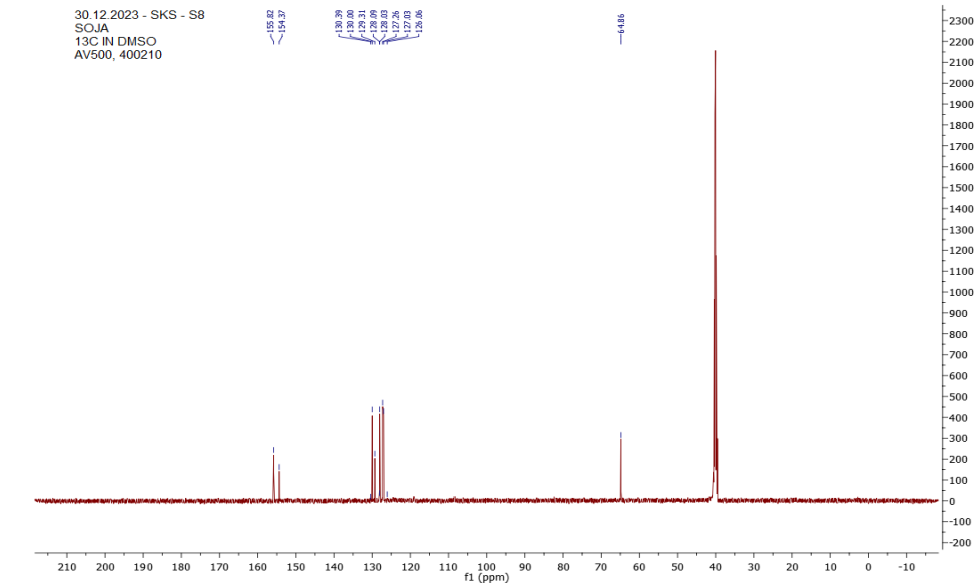

Figure 35: ^{13}C NMR Spectra for compound S8

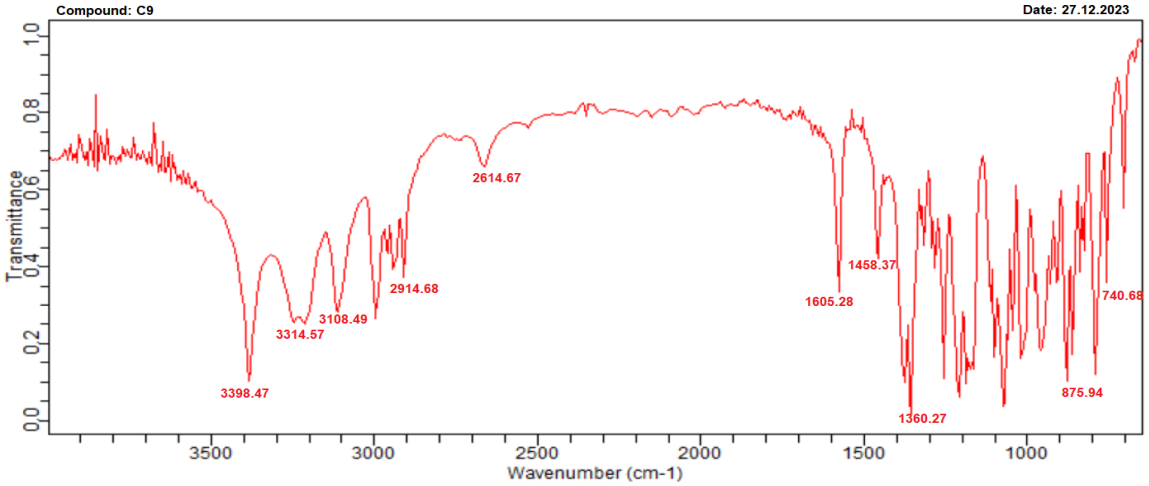

Figure 36: IR Spectra for compound S9

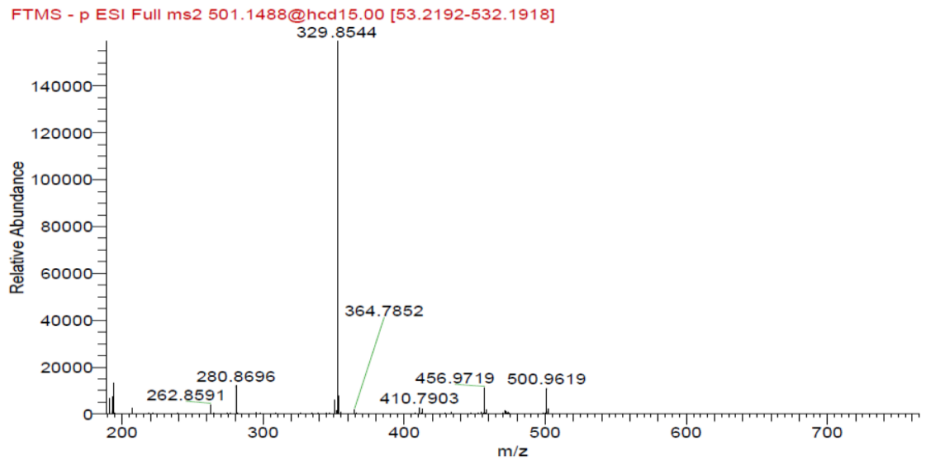

Figure 37: Mass Spectra for compound S9

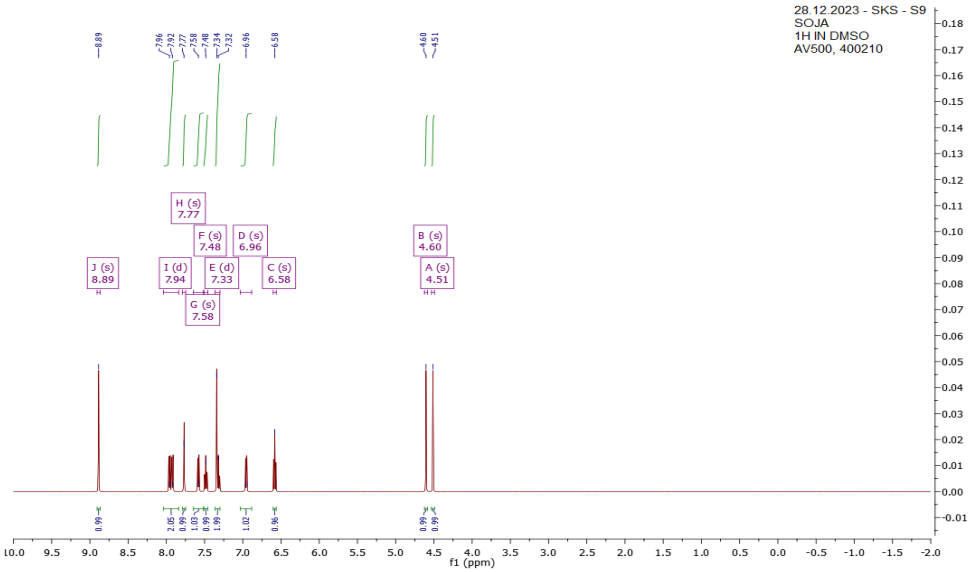

Figure 38: ^{1}H NMR Spectra for compound S9

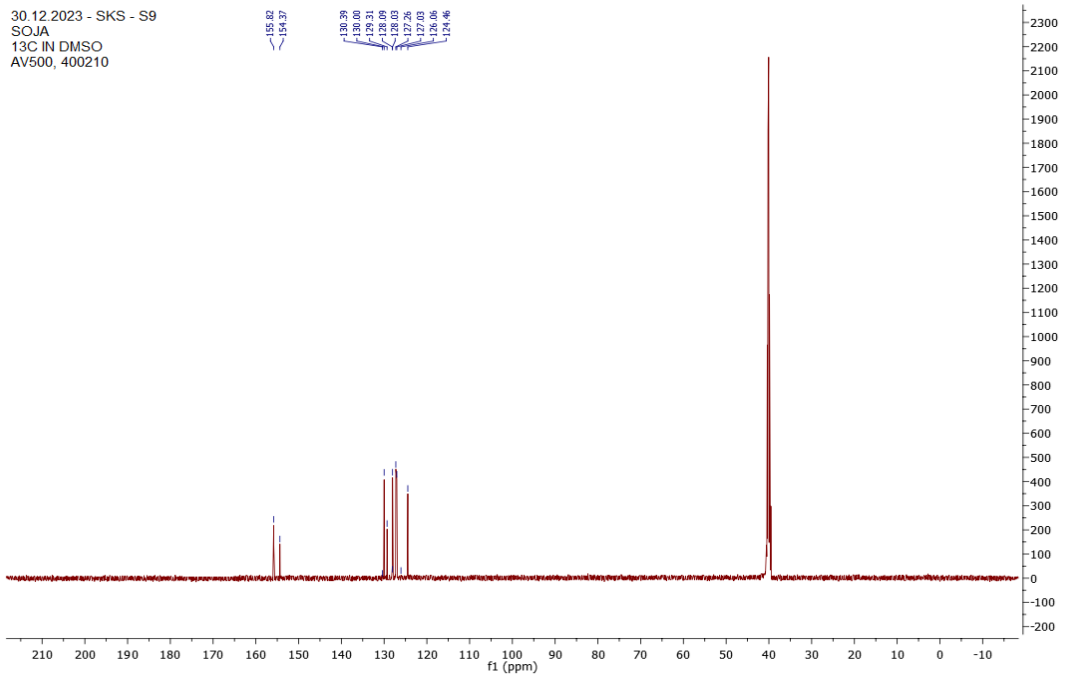

Figure 39: ^{13}C NMR Spectra for compound S9

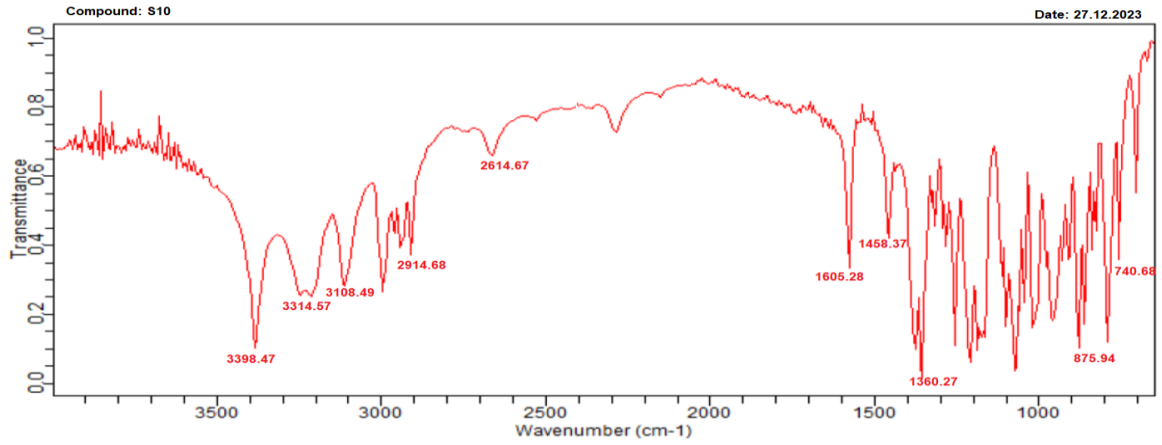

Figure 40: IR Spectra for compound S10

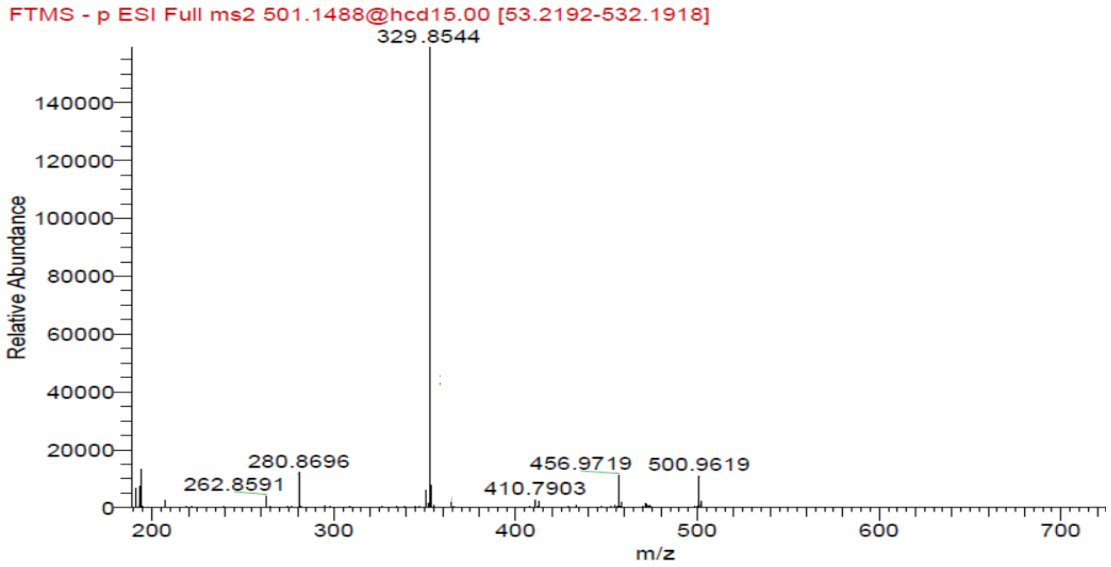

Figure 41: Mass Spectra for compound S10

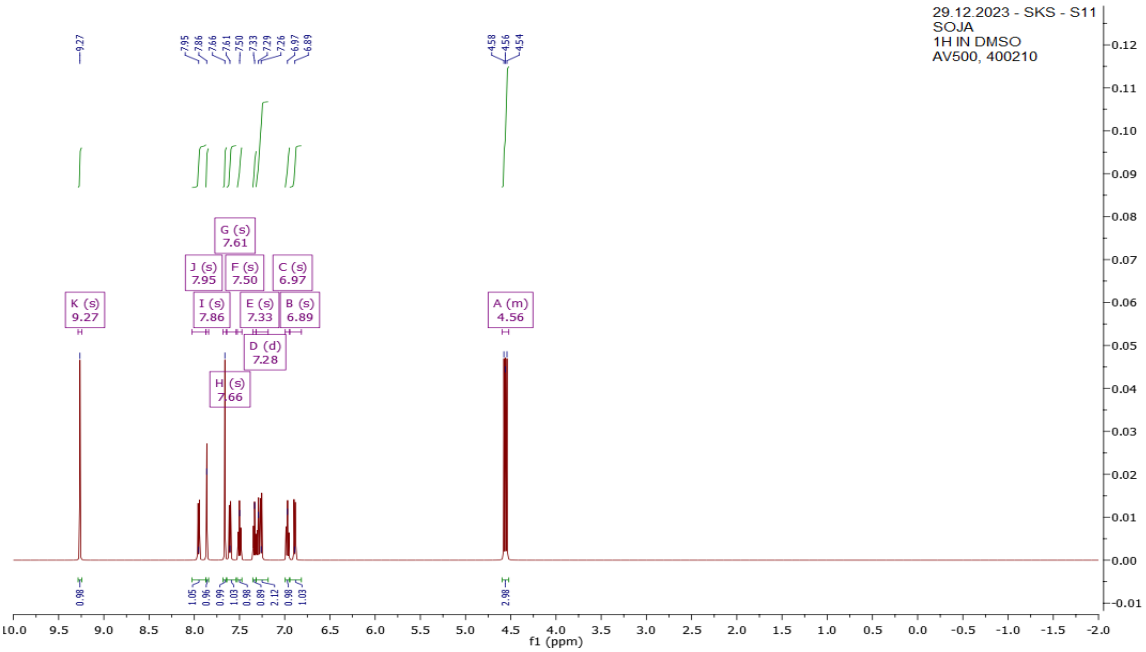

Figure 42: ^{1}H NMR Spectra for compound S10

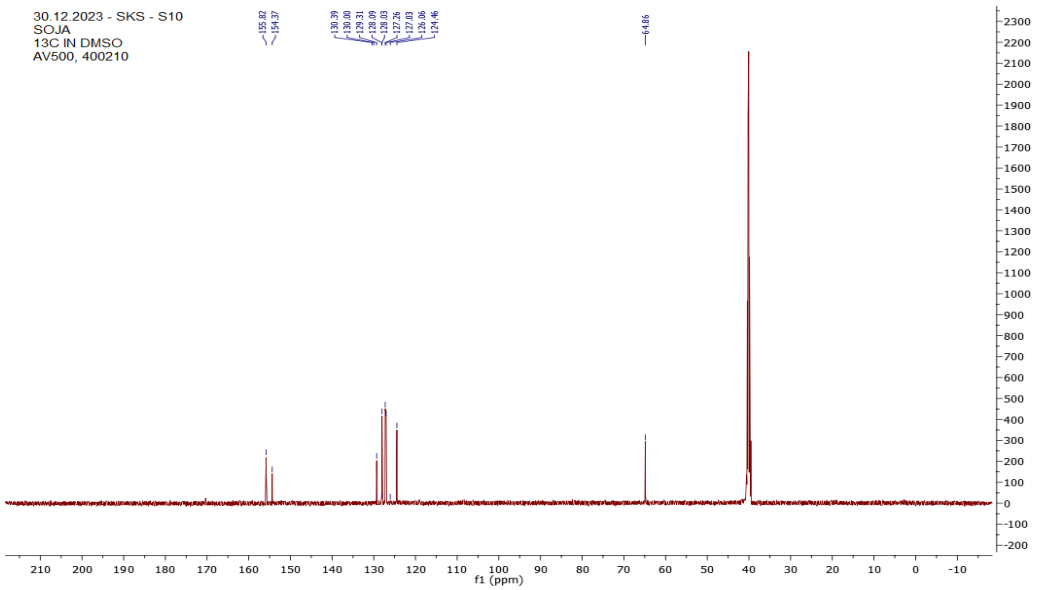

Figure 43: ^{13}C NMR Spectra for compound S10

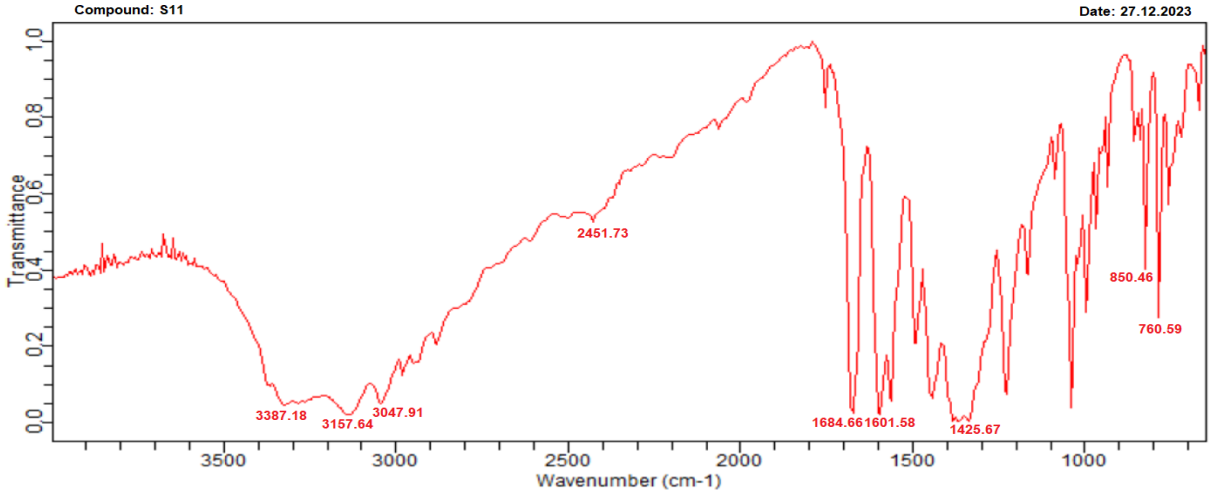

Figure 44: IR Spectra for compound S11

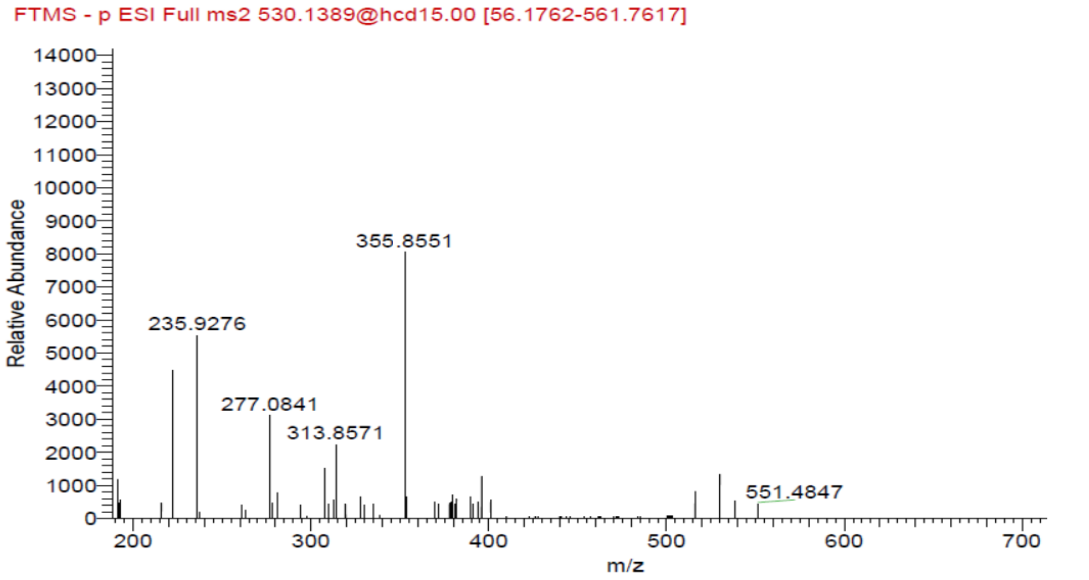

Figure 45: Mass Spectra for compound S11

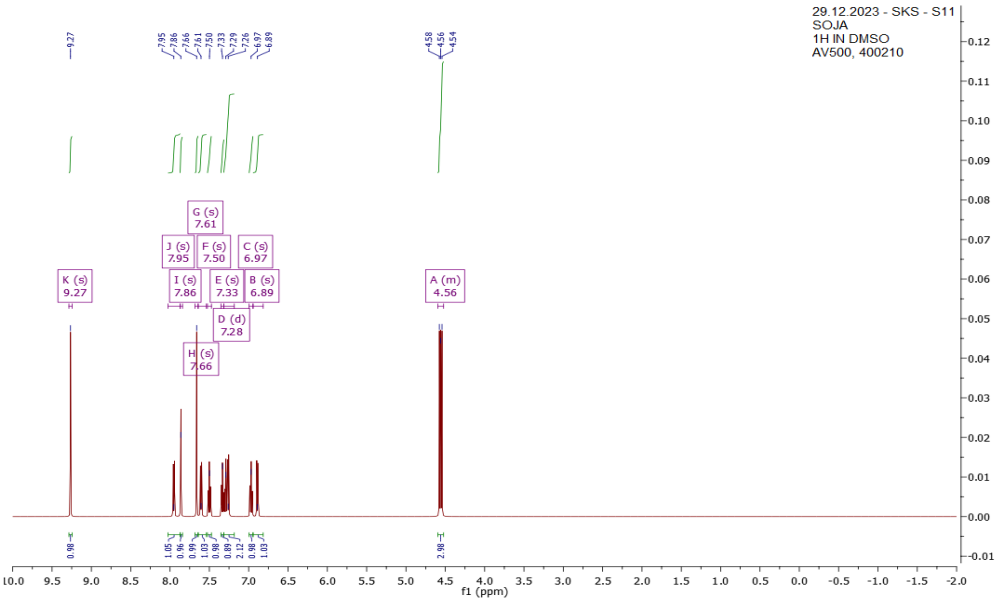

Figure 46: [1]H NMR Spectra for compound S11

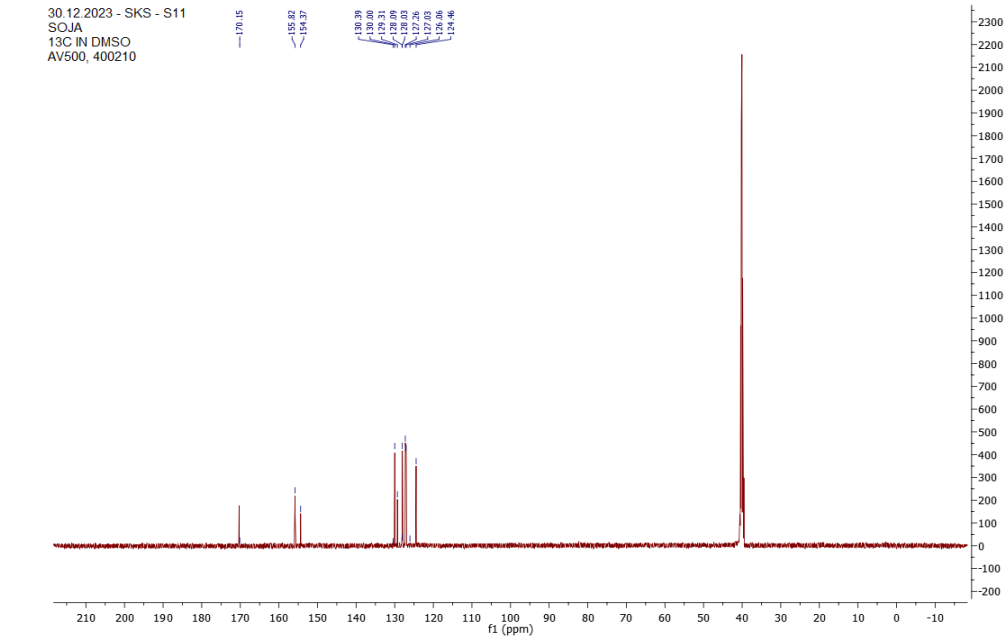

Figure 47: [13]C NMR Spectra for compound S11

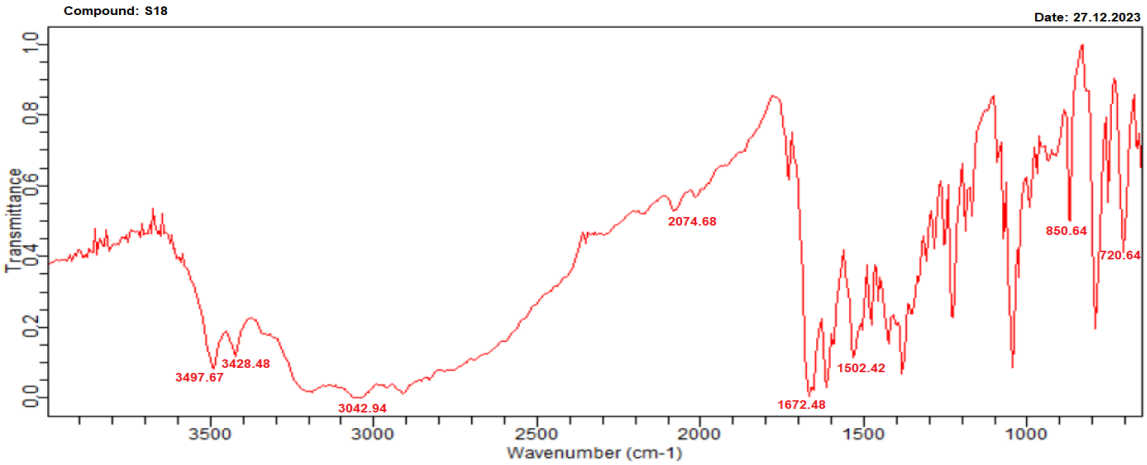

Figure 48: IR Spectra for compound S18

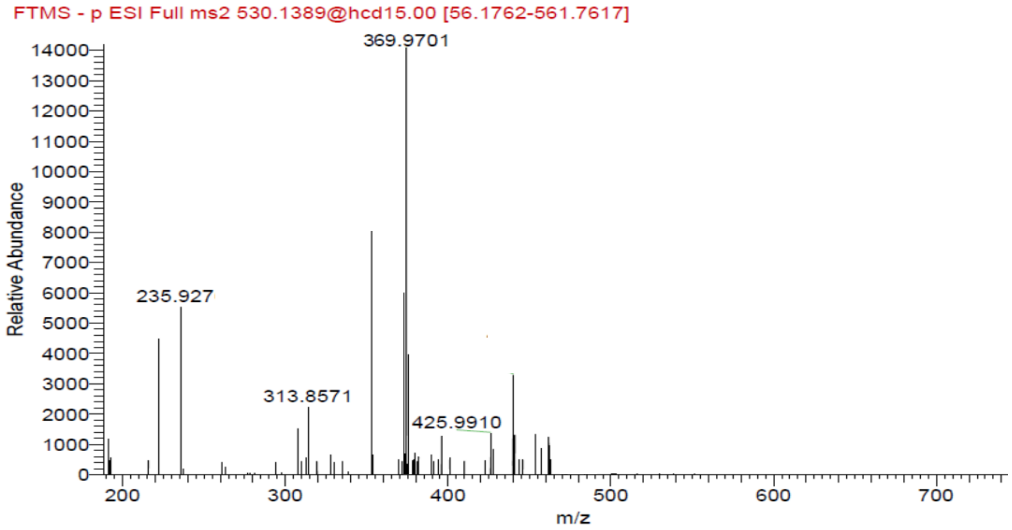

Figure 49: Mass Spectra for compound S18

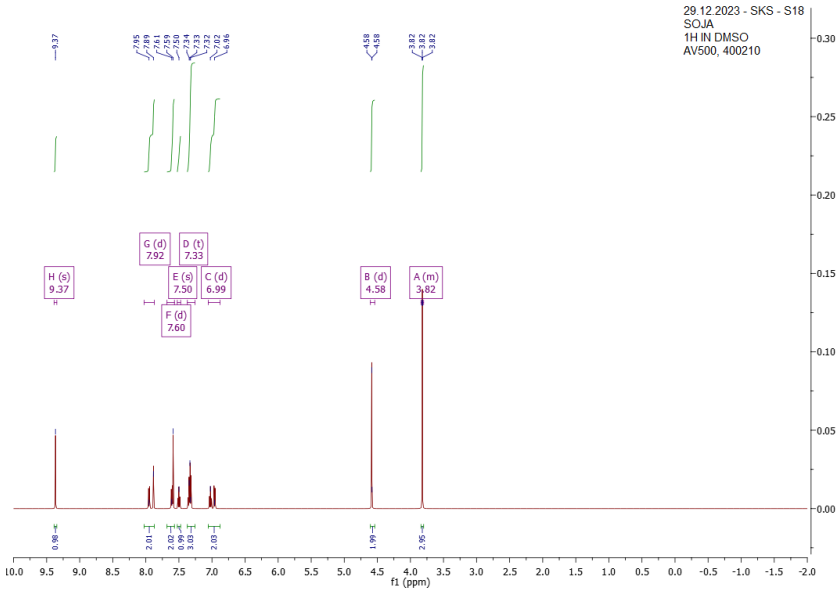

Figure 50: ^{1}H NMR Spectra for compound S18

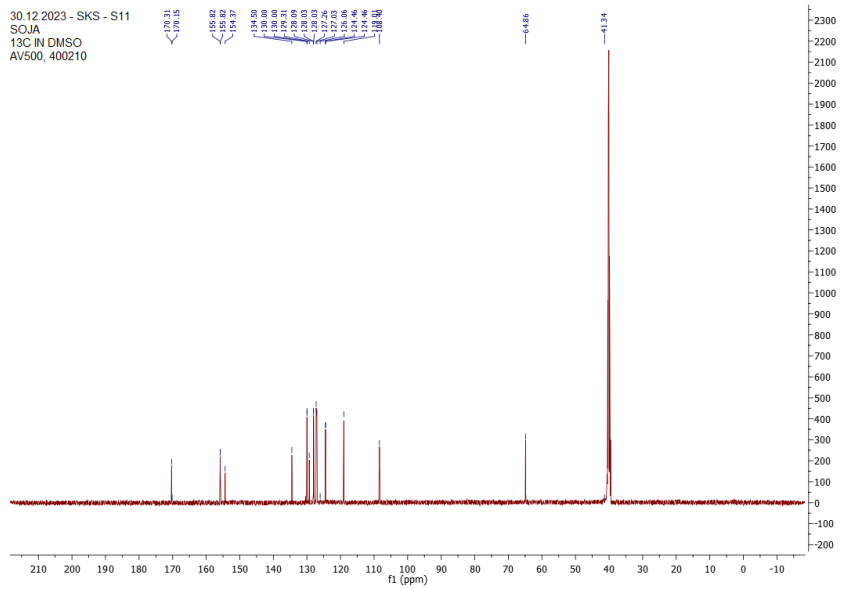

Figure 51: ^{13}C NMR Spectra for compound T18

Characterization of synthesized compounds

(E)-1-((2-chloroquinolin-3-yl)methyl)-3-(4-fluorobenzylidene)thiourea (S2)

$C_{18}H_{13}ClFN_3S$; Yellow colour solid; MP: 110 – 113^{O}C; yield: 69%; Rf: 0.54; IR (KBr) cm^{-1}: 3495 (NH str amine),3030 (CH str CH=CH), 2985 (CH str CH_2), 2124 (CH str aromatic), 1493 (C-N bending), 850 (Aromatic ring), 730 (C-Cl str); ^{1}H NMR (500 MHz, DMSO) δ 9.17 (s, 4H), 7.95 (s, 4H), 7.82 (s, 4H), 7.56 (s, 5H), 7.48 (s, 3H), 7.38 – 7.34 (m, 8H), 7.31 (s, 4H), 7.29 – 7.23 (m, 8H), 6.89 (s, 4H), 4.62 (s, 4H), 4.43 (s, 4H); ^{13}C NMR (101 MHz, DMSO) δ 167.80, 166.81, 135.51, 134.35, 133.35, 132.10, 131.19, 129.76, 129.72, 129.05. Mass: Actual: 357 m/z; Found: 357 m/z.

(E)-1-((2-chloroquinolin-3-yl)methyl)-3-(4-methylbenzylidene)thiourea (S3)

$C_{19}H_{16}ClN_3S$; Yellow colour solid; MP: 104 – 107^{O}C; yield: 71%; Rf: 0.59; IR (KBr) cm^{-1}: 3320 (NH str amine), 3021 (CH str CH=CH), 2950 (CH str CH_2), 2154 (CH str aromatic), 1403 (C-N bending), 850 (Aromatic ring), 720 (C-Cl str) ; ^{1}H NMR (500 MHz, DMSO) δ 9.37 (s, 1H), 7.95 (dd, *J* = 7.5, 1.4 Hz, 1H), 7.88 (d, *J* = 1.4 Hz, 1H), 7.61 (dt, *J* = 7.5, 1.4 Hz, 1H), 7.50 (td, *J* = 7.5, 1.5 Hz, 1H), 7.44 – 7.37 (m, 3H), 7.34 (td, *J* = 7.5, 1.5 Hz, 1H), 7.25 (d, *J* = 7.5 Hz, 2H), 4.63 (s, 1H), 4.54 (s, 1H), 2.35 (s, 3H); ^{13}C NMR (101 MHz, DMSO) δ 167.80, 167.41, 166.81, 135.51, 134.67, 134.35, 133.35, 132.10, 131.19, 130.08, 129.76, 129.72, 129.05, 18.74; Mass: Actual: 353; Found:352 m/z (M-1) .

(E)-1-(4-aminobenzylidene)-3-((2-chloroquinolin-3-yl)methyl)thiourea (S5)

$C_{18}H_{15}ClN_4S$; off white colour solid; MP: 115 – 117^{O}C; yield: 61%; Rf: 0.64; IR (KBr) cm^{-1}: 3350 (NH str amine), 3008 (CH str CH=CH), 2824 (CH str CH_2), 2210 (CH str aromatic), 1425 (C-N bending), 820 (Aromatic ring), 730 (C-Cl str); ^{1}H NMR (500 MHz, DMSO) δ 9.31 (s, 1H), 7.95 (dd, *J* = 7.5, 1.4 Hz, 1H), 7.88 (d, *J* = 1.4 Hz, 1H), 7.61 (dt, *J* = 7.5, 1.4 Hz, 1H), 7.50 (td, *J* = 7.5, 1.5 Hz, 1H), 7.39 – 7.26 (m, 4H), 6.78 (d, *J* = 7.5 Hz, 2H), 4.63 (s, 1H), 4.54 (s, 1H), 4.43 (s, 2H); ^{13}C NMR (101 MHz, DMSO) δ 167.80, 167.41, 166.81, 135.51, 134.67, 134.35, 133.35, 132.10, 131.19, 130.08, 129.76, 129.72, 129.05; Mass: Actual: 354; Found: 354 m/z.

(E)-1-((2-chloroquinolin-3-yl)methyl)-3-(pyridin-2-ylmethylene)thiourea (S6)

$C_{17}H_{13}ClN_4S$; white colour solid; MP: 106 – 109^{O}C; yield: 63%; Rf: 0.59; IR (KBr) cm^{-1}:3300 (NH str amine), 3071 (CH str CH=CH), 2950 (CH str CH2), 2408 (CH str aromatic), 1435 (C-N bending), 850 (Aromatic ring), 720 (C-Cl str) ; ^{1}H NMR (500 MHz, DMSO) δ 8.94 (s, 1H), 8.74 (s, 1H), 7.92 (dd, *J* = 28.4, 8.5 Hz, 4H), 7.59 (d, *J* = 16.3 Hz, 2H), 7.50 (s, 1H), 7.45 (s, 1H), 7.34 (s, 1H), 4.61 (s, 1H), 4.52 (s, 1H); ^{13}C NMR (101 MHz, DMSO) δ 155.07, 154.08, 138.95, 138.14, 130.38, 129.22, 128.95, 127.82, 126.99, 125.18, 121.74, 120.89; Mass: Actual: 340; Found: 340 m/z.

(E)-1-((2-chloroquinolin-3-yl)methyl)-3-(pyridin-4-ylmethylene)thiourea (S7)

$C_{17}H_{13}ClN_4S$; white colour solid; MP: 115 – 119^{O}C; yield: 62%; Rf: 0.57; IR (KBr) cm^{-1}: 3300 (NH str amine), 3071 (CH str CH=CH), 2950 (CH str CH_2), 2408 (CH str aromatic), 1435 (C-N bending), 850 (Aromatic ring), 720 (C-Cl str) ; ^{1}H NMR (500 MHz, DMSO) δ 8.94 (s, 1H), 8.74 (s, 1H), 7.92 (dd, *J* = 28.4, 8.5 Hz, 4H), 7.59 (d, *J* = 16.3 Hz, 2H), 7.50 (s, 1H), 7.45 (s, 1H), 7.34 (s, 1H), 4.61 (s, 1H), 4.52 (s, 1H); ^{13}C NMR (101 MHz, DMSO) δ 155.07, 154.08, 138.95, 138.14, 130.38, 129.22, 128.95, 127.82, 126.99, 125.18, 121.74, 120.89; Mass: Actual: 340; Found: 340 m/z.

(E)-1-((1H-pyrrol-2-yl)methylene)-3-((2-chloroquinolin-3-yl)methyl)thiourea (S8)

$C_{16}H_{13}ClN_4S$; Brown colour solid; MP: 121 – 123^{O}C; yield: 64%; Rf: 0.53; IR (KBr) cm^{-1}: 3398 (NH str amine), 3030 (CH str CH=CH), 2984 (CH str CH_2), 2354 (CH str aromatic), 1400 (C-N bending), 850 (Aromatic ring), 740 (C-Cl str); ^{1}H NMR (500 MHz, DMSO) δ 9.12 (s, 1H), 7.92 (s, 1H), 7.78 (s, 1H), 7.56 (d, *J* = 16.4 Hz, 2H), 7.48 (s, 1H), 7.37 (s, 1H), 7.32 (s, 1H), 7.07 (s, 1H), 6.76 (s, 1H), 6.42 (s, 1H), 4.56 (d, *J* = 2.6 Hz, 2H); ^{13}C NMR (126 MHz, DMSO) δ 155.82, 154.37, 130.39, 130.00, 129.31, 128.09, 128.03, 127.26, 127.03, 124.46, 64.86; Mass: Actual: 328; Found: 328 m/z.

E)-1-((2-chloroquinolin-3-yl)methyl)-3-(furan-2-ylmethylene)thiourea (S9)

$C_{16}H_{12}ClN_3OS$; White colour solid; MP: 122 – 124^{O}C; yield: 61%; Rf: 0.56; IR (KBr) cm^{-1}: 3398 (NH str amine), 3108 (CH str CH=CH), 2914 (CH str CH_2), 2614 (CH str aromatic), 1493 (C-N bending), 875 (Aromatic ring), 740 (C-Cl str) ; ^{1}H NMR (500 MHz, DMSO) δ 8.89 (s, 1H), 7.94 (d, *J* = 18.9 Hz, 2H), 7.77 (s, 1H), 7.58 (s, 1H), 7.48 (s, 1H), 7.33 (d, *J* = 10.8 Hz, 2H), 6.96 (s, 1H), 6.58 (s, 1H), 4.60 (s, 1H), 4.51 (s,

1H); ^{13}C NMR (126 MHz, DMSO) δ 155.82, 154.37, 130.39, 130.00, 129.31, 128.09, 128.03, 127.26, 127.03, 126.06, 124.46; Mass: Actual: 329; Found: 329 m/z.

(E)-1-((1H-imidazol-2-yl)methylene)-3-((2-chloroquinolin-3-yl)methyl)thiourea (S10)
$C_{15}H_{12}ClN_5S$; Orange colour solid; MP: 125 - 127^{O}C; yield: 61%; Rf: 0.51; IR (KBr) cm^{-1}:3398 (NH str amine), 3108 (CH str CH=CH), 2914 (CH str CH_2), 2614 (CH str aromatic), 1458 (C-N bending), 875 (Aromatic ring), 740 (C-Cl str) ; ^{1}H NMR (500 MHz, DMSO) δ 8.95 (s, 2H), 7.93 (d, *J* = 9.6 Hz, 4H), 7.77 (s, 2H), 7.54 (d, *J* = 35.5 Hz, 3H), 7.48 (s, 3H), 7.32 (s, 2H), 7.03 (s, 2H), 6.76 (s, 2H), 4.55 (d, *J* = 12.2 Hz, 4H); ^{13}C NMR (126 MHz, DMSO) δ 155.82, 154.37, 130.39, 130.00, 129.31, 128.09, 128.03, 127.26, 127.03, 126.06, 124.46, 64.86; Mass: Actual: 329; Found: 329 m/z.

(E)-1-((2-chloroquinolin-3-yl)methyl)-3-(2-hydroxybenzylidene)thiourea (S11)
$C_{18}H_{14}ClN_3OS$; White colour solid; MP: 115 - 117^{O}C; yield: 74%; Rf: 0.61; IR (KBr) cm^{-1}:3387 (NH str amine), 3047 (CH str CH=CH), 2985 (CH str CH_2), 2451 (CH str aromatic), 1425 (C-N bending), 850 (Aromatic ring), 760 (C-Cl str) ; ^{1}H NMR (500 MHz, DMSO) δ 9.27 (s, 1H), 7.95 (s, 1H), 7.86 (s, 1H), 7.66 (s, 1H), 7.61 (s, 1H), 7.50 (s, 1H), 7.33 (s, 1H), 7.28 (d, *J* = 15.2 Hz, 2H), 6.97 (s, 1H), 6.89 (s, 1H), 4.60 – 4.52 (m, 3H); ^{13}C NMR (126 MHz, DMSO) δ 155.82, 155.82, 154.37, 134.50, 130.39, 130.00, 130.00, 129.31, 128.09, 128.03, 128.03, 127.26, 127.03, 126.06, 124.46, 124.46, 119.01, 108.40, 64.86; Mass: Actual: 355; Found: 355 m/z.

(E)-1-((2-chloroquinolin-3-yl)methyl)-3-(2-methoxybenzylidene)thiourea (S18)
$C_{19}H_{16}ClN_3OS$; White colour solid; MP: 123 - 127^{O}C; yield: 62%; Rf: 0.50; IR (KBr) cm^{-1}:3428 (NH str amine), 3042 (CH str CH=CH), 2074 (CH str aromatic), 1502 (C-N bending), 850 (Aromatic ring), 720 (C-Cl str) ; ^{1}H NMR (500 MHz, DMSO) δ 9.27 (s, 1H), 7.95 (s, 1H), 7.86 (s, 1H), 7.66 (s, 1H), 7.61 (s, 1H), 7.50 (s, 1H), 7.33 (s, 1H), 7.28 (d, *J* = 15.2 Hz, 2H), 6.97 (s, 1H), 6.89 (s, 1H), 4.60 – 4.52 (m, 3H); ^{13}C NMR (126 MHz, DMSO) δ 170.31, 170.15, 155.82, 155.82, 154.37, 134.50, 130.39, 130.00, 130.00, 129.31, 128.09, 128.03, 128.03, 127.26, 127.03, 126.06, 124.46, 124.46, 119.01, 108.40, 64.86, 41.34; Mass: Actual: 369; Found: 369 m/z.

MTT assay for cell viability
The MTT test was utilized to gauge cell viability. The cells were plated in a 96-well plate with 1 104 cells per well which were determined by reading the control and plotting a logarithmic graph of the percentage of cell viability Vs sample concentration. Averaging the results of the triple trials allowed for the determination of the final concentration that yields the maximum viability. For the in vitro cytotoxicity examination, the MTT assay method was applied to human SH-SY5Y neuroblastoma cells. All of the medications under investigation have improved survival of more than 70% at concentration 500nm. Among the tested compounds, the derivative S9substituted with highly electronegative atom Cl and oxygen containing ring shows promising viability 80.27% at the concentration range 500 nm, followed by the compound S11substituted with electronegative atoms like OH and Cl atom shows good percentage viability 78.64% at 500 nm, against the tested cell line Human SH-SY5Y neuroblastoma. Based on the results it's clearly showed that, the electronegative atom may alter the biological activity of the compounds in tested cell lines.

Table 4. Results for *in vitro* MTT assay of cell viability of the compounds

Compound	% viability
S2	73.24
S3	74.21
S5	69.27
S6	69.51
S7	71.51
S8	74.38
S9	80.27
S10	74.36
S11	78.64
S18	64.27

SUMMARY AND CONCLUSION:

The structure of the newly synthesized compounds was validated by physical, chemical, and spectroscopic data. In molecular docking studies, the studied drugs demonstrated a similar mechanism of protein binding to the active region of the acetyl cholinesterase protein (PDB ID:1F8U). According on the predicted docking energies, the interaction with cholinesteraseenzyme is shows promising binding energy. All substances were tested for viability in vitro against Human SH-SY5Y neuroblastoma cell lines. Compounds S9 and S11 were shown to be the most effective against the evaluated cell lines. Work is being done to advance the search for new cholinesterase inhibitors. In order to establish a SAR for rational study, more derivatives and in-depth, detailed investigations on in vivo activity may be undertaken. The current study suggests that more research is needed forquinoline derivatives developed as a potent lead for Alzheimer's disease.

ACKNOWLEGDE:

I would like to express my special thanks to the mentor and department of chemistry people for there time and efforts they provided throughout the year.Your useful advice and suggestions were really helpful to me during the project completion.

CONFLICT OF INTEREST:

The author has no conflict of interest.

REFERNCE:

1. Albert AA, Andrea C, Roberto N, Aydie H, Emidio C, Jordi M, Roberto P, Antonio M, “Exploring the effect of PARP-1 flexibility in docking studies”, Journal of Molecular Graphics and Modelling, 45, (2013): 192 –201
2. .Roko Z, Andreja M, Eva B, Ivan A, “Molecular Insights into Poly(ADP-ribose) Recognition and Processing:,Biomolecules, 3 (2013): 1- 17
3. Julio CM, Longshan L, Farjana JF, Ying D, Erik AB, Malina P, Jinming G, David AB, “Review of Poly (ADP-ribose) Polymerase (PARP) Mechanisms of Action and Rationale for Targeting in Cancer and Other Diseases” Critical Reviews TM in Eukaryotic Gene Expression, 24 no. 1, (2014): 15 - 28.
4. Elizabeth Eldhose, Gowrmma B, Manal Mohammed, Kalirajan R, Kavarasan L, “Translational chemotherapy for triple negative breast cancer -A review on significance of poly (ADP-ribose) polymerase 1 (PARP1) inhibitors”. Research Journal of Pharmacy and Technology. 12 no. 6, (2019): 1-7.
5. Rupinder KS, Nirmal S, Amteshwar SJ, “Poly(ADP-ribose) polymerase-1 (PARP-1) and its therapeutic implications”. Vascular Pharmacology, 53, (2010): 77–87.
6. Kaviarasan L, Elizabeth E, Praveen TK, Kalirajan R, Manal M, Pulla Prudviraj and Gowramma B, “1,3,4-Thiadiazolo (3,2-A) Pyrimidine-6-Carbonitrile Scaffold as PARP1 Inhibitor”, Anti-Cancer Agents in Medicinal Chemistry, 21, (2021): 1-16.
7. Hui L, Yan H, Xueyan W, Guangwei H, Yungen X, Qihua Z, “Novel tricyclic poly (ADP-ribose) polymerase-1/2 inhibitors with potent anticancer chemopotentiating activity: Design, synthesis and biological evaluation”. Bioorganic & Medicinal Chemistry, 24, (2016): 4731–4740.
8. Kovi KE, Yearick K, Iwaniuk DP, Natarajan JK, Alumasa J, de Dois AC, Roepe PD, Wolf C, “Search for new pharmacophores for antimalarial activity. Part I: synthesis and antimalarial activity of new 2-methyl-6-ureido-4-quinolinamides” Bioorg. Med. Chem, 17, (2009): 270–283.
9. Snider DE, Raviglione M Jr, Kochi A. Global burden of tuberculosis, chapter 1. In: Tuberculosis:Pathogenisis, Protection, and Control. American society for Microbiology, Washington, DC 20005.1994:3–11.
10. El-Shorbagi AN, Chaudhary S, Alshemali KA, et al. A comprehensive review on management of Parkinson’s disease, inclusive of drug discovery and pharmacological approaches. J Appl Pharm Sci 2020; 10: 130–150.
11. Subramanian G, Chand J, Jupudi S, et al. Synthesis and Biological Evaluation of the Selected Naphthalene Substituted Azetidinone Derivatives Targeting Parkinson’s Disease. Indian J Pharm Educ Res 2023; 57: 552– 558.

12. Cheong SL, Federico S, Spalluto G, et al. The current status of pharmacotherapy for the treatment of Parkinson's disease: transition from single-target to multitarget therapy. Drug Discov Today 2019; 24: 1769– 1783.
13. Zhang Y, Xu X. Chinese Herbal Medicine in the Treatment of Depression in Parkinson's Disease: From Molecules to Systems. Front Pharmacol 2022; 13.
14. Dorszewska J, Kowalska M, Prendecki M, et al. Oxidative stress factors in Parkinson's disease. Neural RegenRes 2021; 16: 1383–1391. doi:10.4103/1673-5374.300980
15. Sawa K, Uematsu T, Korenaga Y, et al. Krebs cycle intermediates protective against oxidative stress bymodulating the level of reactive oxygen species in neuronal HT22 cells. Antioxidants 2017; 6.
16. Shen Y, Wu Q, Shi J, et al. Regulation of SIRT3 on mitochondrial functions and oxidative stress in Parkinson's disease. Biomed Pharmacother 2020; 132: 110928.
17. Lagouge M, Argmann C, Gerhart-Hines Z, et al. Resveratrol Improves Mitochondrial Function and Protectsagainst Metabolic Disease by Activating SIRT1 and PGC-1α. Cell 2006; 127: 1109–1122.
18. Zhang B, Zhai M, Li B, et al. Honokiol ameliorates myocardial ischemia/reperfusion injury in type 1 diabeticrats by reducing oxidative stress and apoptosis through activating the SIRT1-Nrf2 signaling pathway. OxidMed Cell Longev 2018; 2018.
19. Baeken MW, Schwarz M, Kern A, et al. The selective degradation of sirtuins via macroautophagy in theMPP+ model of Parkinson's disease is promoted by conserved oxidation sites. Cell Death Discov 2021; 7.
20. Zang H, Yang W, Tian X. Simvastatin in the Treatment of Colorectal Cancer : A Review. 2022.
21. Jia CY, Li JY, Hao GF, et al. A drug-likeness toolbox facilitates ADMET study in drug discovery. DrugDiscov Today 2020; 25: 248–258. doi:10.1016/j.drudis.2019.10.014
22. Zhang J, Xiang H, Liu J, et al. Mitochondrial Sirtuin 3: New emerging biological function and therapeutictarget. Theranostics 2020; 10: 8315–8342. doi:10.7150/thno.45922
23. Chen Y, Fu LL, Wen X, et al. Sirtuin-3 (SIRT3), a therapeutic target with oncogenic and tumor-suppressivefunction in cancer. Cell Death Dis 2014; 5: 1–7.
24. Lu J, Zhang H, Chen X, et al. A small molecule activator of SIRT3 promotes deacetylation and activation ofmanganese superoxide dismutase. Free Radic Biol Med 2017; 112: 287–297.
25. El Faydy M, Dahaieh N, Ounine K, et al. Synthesis, Identification, Antibacterial Activity, ADME/T and DNA-Docking Investigations of 8-Quinolinol Analogs Bearing a Benzimidazole Moiety. Arab J Sci Eng2022; 47: 497–510. doi:10.1007/s13369-021-05749-7
26. Hasan MM, Khan Z, Chowdhury MS, et al. In silico molecular docking and ADME/T analysis of Quercetincompound with its evaluation of broad-spectrum therapeutic potential against particular diseases. InformaticsMed Unlocked 2022; 29: 100894. doi:10.1016/j.imu.2022.100894
27. Ajiboye BO, Fagbola TM, Folorunso IM, et al. In silico identification of chemical compounds in Spondiasmombin targeting aldose reductase and glycogen synthase kinase 3β to abate diabetes mellitus. InformaticsMed Unlocked 2023; 36: 101126.
28. Ahmad F. Ganoderic Acid A targeting leucine-rich repeat kinase 2 involved in Parkinson's disease–Acomputational study. Aging Med 2023; 6: 272–280.
29. Ranade SD, Alegaon SG, Venkatasubramanian U, et al. Design, synthesis, molecular dynamics simulation,MM/GBSA studies and kinesin spindle protein inhibitory evaluation of some 4-aminoquinoline hybrids.Comput Biol Chem 2023; 105: 107881.
30. Synthesis of novel quinoline-based thiadiazole, evaluation of their antileishmanialpotential and molecular docking studies – ScienceDirecthttps://www.sciencedirect.com/science/article/abs/pii/S0045206818301044 (accessed2021 -12 -26).
31. A. Atri, L. Frölich, C. Ballard, PN. Tariot, JL. Molinuevo, N. Boneva, K. Windfeld, LL. Raket, and JL. Cummings. Effect of Idalopirdine as Adjunct to Cholinesterase Inhibitors on Change in Cognition in Patients with Alzheimer Disease: Three Randomized Clinical Trials. JAMA, 2018; 319: 130–142.